Journal of Asian Earth Sciences 259 (2024) 105869

Contents lists available at ScienceDirect

Journal of Asian Earth Sciences

journal homepage: www.elsevier.com/locate/jseaes

The boundary between the Middle and Upper Cambrian strata in the Tarim Basin, NW China: Regional to global SPICE event correlation

Yaxin Shang [a], Keyu Liu [a,*], Zhiqian Gao [b,c,*], Chenjia Zhang [d], Ziyi Wang [a]

[a] School of Geosciences, China University of Petroleum, Qingdao 266580, China
[b] School of Energy Resource, China University of Geosciences, Beijing, China
[c] Key Laboratory of Marine Reservoir Evolution and Hydrocarbon Enrichment Mechanisms, Ministry of Education, China University of Geosciences, Beijing, China
[d] School of Earth Sciences and Engineering, Nanjing University, Nanjing, China

ARTICLE INFO

Keywords:
Middle-Upper Cambrian boundary
Unconformity
Carbon isotope excursion
Tarim Basin
SPICE

ABSTRACT

The subdivision and correlation of the Cambrian System have long been controversial globally with multiple schemes. This is especially the case for the Tarim Basin, western China where regional and global correlations of the Middle-Upper Cambrian boundary are hampered by incomplete biostratigraphy. The Middle-Upper Cambrian boundary (T_8^1) in the Tarim Basin is characterized by an abrupt switch of lithological and sedimentary facies, a sudden change of wireline log responses, and the contrasting seismic features, structural styles and carbonate platform architectures. The T_8^1 boundary manifests in various forms and styles including *syn*-sedimentary unconformity, overlapping unconformity, tectonic unconformity, multi-stage superimposed unconformity, parallel unconformity and conformity. Each manifestation type of the T_8^1 boundary was influenced by at least one of the factors including paleo-geomorphology, tectonic movement, eustacy, and climatic change. Based on the correlation between carbon isotopes and sedimentary characteristics in different regions globally, we suggest that the $\delta^{13}C$ weak negative shift that follows the strongly positive shift of the Late Cambrian SPICE event can serve as a reliable isotope stratigraphic marker for identifying the T_8^1 boundary of the western Tarim Platform. The top of the Awatag Formation (the top of the Middle Cambrian) in the western Tarim Platform should thus be correlated to the top of the Mohershan Formation in the eastern Tarim Basin, corresponding to the top of the Miaolingian Stage. The absence of the SPICE event in the western part of the Tarim Basin may have been caused by a regional depositional hiatus associated with the T_8^1 boundary.

1. Introduction

Stratigraphic boundary, by definition, is a stratigraphic surface that separates older strata units below from younger formations above, containing biostratigraphic, chronostratigraphic, paleogeographic, contact-relationship, and sequence-stratigraphic information (Hintze and Robison, 1975; Li et al., 2017a; Zhu et al., 2006; Robison, 1982, 1999). Therefore, at least in part, stratigraphic boundaries can serve as system tracts or sequence boundaries when constructing a chronostratigraphic framework for regional or even global correlations (Carter et al., 1998; Van Wagoner et al., 1990). Cambrian is the first period of the Phanerozoic Eon, witnessed both biological thriving and a mass extinction. It was a period exhibiting a rapid shift of the earth-life system from dominantly microbial forms to a predominance of taxonomically diverse multicellular organisms (Maruyama et al., 2014; Shahkarami et al., 2020), referred to as the Cambrian "life explosion", and is regarded as a pivotal period in life evolution on Earth (Darroch et al., 2018; Wu et al., 2021). In 2004, the International Subcommission on Cambrian Stratigraphy (ISCS) proposed a division of the Cambrian System into "four series and ten stages," a classification that has since been broadly accepted within the geological community (Geyer and Shergold, 2000; Babcock et al., 2005; Peng et al., 2006). However, the Cambrian chronostratigraphy of the Western Tarim Basin in western China currently adheres to a different subdivision, consisting of "three series and six stages" (Zhu et al., 2019a). Therefore, demarcating the boundaries of the Cambrian stratigraphic units and correlating them to the international subdivision standard becomes crucial and timely in studying chronostratigraphy in the Tarim Basin (Yao et al., 2014; Cai et al., 2014).

In studying the Cambrian stratigraphic boundaries in the Tarim

* Corresponding authors at: School of Energy Resource, China University of Geosciences, Beijing, China (Z. Gao).
E-mail addresses: liukeyu@upc.edu.cn (K. Liu), gzq@cugb.edu.cn (Z. Gao).

https://doi.org/10.1016/j.jseaes.2023.105869
Received 18 February 2023; Received in revised form 18 September 2023; Accepted 25 September 2023
Available online 26 September 2023

Basin, the Ediacaran–Cambrian boundary (Yao et al., 2014; He et al., 2019; Wang et al., 2020a), the Lower–Middle Cambrian boundary (Wang et al., 2011; Gao and Fan, 2015) and the Cambrian–Ordovician boundary have been extensively investigated (Lin et al., 2012; Wang et al., 2017a). In comparison, the Middle–Upper Cambrian boundary in the Tarim Basin has been neglected and rarely investigated. Simultaneously, the absence of mega-fossils in the Middle–Upper Cambrian boundary strata in the Tarim Basin, coupled with a lack of biostratigraphic information, results in potential discrepancies during stratigraphic division. Consequently, identifying this Middle–Upper Cambrian boundary and establishing a basin-wide correlation present substantial challenges. Identification of unconformities has long been used as a common method in tracking stratigraphic boundaries and analyzing their key characteristics and genesis (He et al., 2014; Lin et al., 2012). However, since the Middle–Upper Cambrian strata in the eastern Tarim Basin did not develop any major unconformities, better methods are needed to identify and compare this boundary over the entire basin.

Over the last two decades, with the advancement of isotopic analysis and its increasing application, carbon isotopes have been widely used for stratigraphic correlation and have even been used as the primary tool in defining the base of the Eocene Epoch (of the Paleogene Period) (Allan and Matthes, 1982; Rush and Chafetz, 1990; Saller et al., 1994; Ford and Williams, 2007). The Cambrian Period is characterized by four positive and six negative carbon isotopic prominent excursions in most areas worldwide (Peng et al., 2004a; Babcock et al., 2005; Zhu et al., 2006; Peng et al., 2012). The study of the evolution of $\delta^{13}C$ values in marine carbonate rocks for global stratigraphic correlation and division is an important research topic in the field of earth sciences (Zhu et al., 2019; Wang et al., 2011). One of the positive excursions, the Upper Cambrian Steptoean Positive Carbon Isotope Excursion (SPICE; starting at ca. 497 Ma and lasting for approximately 2–4 Myr), has been documented from palaeocontinents in various settings, including Antarctica, Argentina (Sial et al., 2008, 2013), Australia (Lindsay et al., 2005), France (Wotte et al., 2007), England, Kazakhstan, Laurentia, Newfoundland (Hurtgen et al., 2009), North and South China (Chen et al. 2011, 2012; Ng et al., 2014), Siberia (Kouchinsky et al., 2008), Sweden (Ahlberg et al., 2010), and the USA (Saltzman et al., 1998, 2000, 2011; Gill et al., 2007, 2011; Woods et al., 2011). However, from published data so far, the SPICE excursions have rarely been recorded in the Middle–Upper Cambrian strata in the Tarim Basin (Zhang et al., 2020), especially in the western platform area of the basin. Can the absence of SPICE in most of the western Tarim Basin be regarded as the presence of a depositional hiatus or an unconformity at the base of the Furongian?

Many scholars believed that the bottom of the Yurtus Formation (the base of the Lower Cambrian) corresponds to a significant negative shift in carbon isotopes (the BACE event) (Zhu et al., 2019a; Chen et al., 2020b). Zhu et al. (2006, 2019a) suggested that the base of the Cambrian Stage 5 (Series 3) is close to the termination of the ROECE negative $\delta^{13}C$ excursion, corresponding to the traditional boundary of the Lower/Middle Cambrian series. At the same time, Peng et al. (2004b) and Zhu et al. (2019) suggested that the beginning of the SPICE positive δ13C excursion, which served as a remarkable secondary global marker for the boundary between the Paibian Stage and Guzhuangian Stage, is close to the base of the Furongian Series. Therefore, the prominent issue of why there are so few reported SPICE events in the western part of the Tarim Basin persists in current research.

This study focuses on the boundary between the Awatag and the Xiaqiulitag formations in the Xinjiang region, China, and attempts to achieve the following objectives: (1) formulate methods for identifying the Middle–Upper Cambrian boundary and compare the sedimentary, geochemical and seismic characteristics of the strata below and above the boundary; (2) analyze and classify the contact relationships of the boundary, and evaluate their precise position; (3) examine whether the unconformity was caused by regional tectonics, eustatic sea-level, paleotopography and paleo-tectonics, or composite factors; and (4) identify possible global isotopic events and trends through the Middle–Upper Cambrian transition, thus reinforcing global stratigraphic correlation.

2. Geological setting

The Tarim Basin, covering about 560,000 km^2, is located in northwest China. It is bounded by the Tianshan Mountains to the north, the Kunlun Mountains to the south, the Altyn Tagh Mountains to the southeast (Fig. 1; Tang, 1997; Lin et al., 2009). It is the largest petroliferous basin in China, with huge oil and gas development potential (Li et al., 1996; Nishidai and Berry, 1990; Zhang and Huang, 2005; Zheng et al., 2007).

The Middle–Upper Cambrian in the Tarim Basin presents a sedimentary pattern in which the western part was dominated by a carbonate platform while the eastern part developed as a basin (Chen et al., 2015) (Fig. 1a). The lithostratigraphic subdivision in the western Tarim carbonate platform adopts the same scheme as the outcrop in the Keping area, which is traditionally divided into “three series and six stages” (Yang et al., 2021a). The Lower Cambrian includes the Yuertusi, Xiaoerbulak, and Wusongger formations. The Yuertusi Formation is composed of high-quality source rocks (Fig. 1c). The lithology of the Xiaoerbulak Formation can be divided into two sections. The lower section primarily consists of micritic limestone, while the upper section is largely composed of algal detrital limestone (Fig. 1c). The Middle Cambrian, including the Shayilik and Awatag formations, comprises gypsum layers and is generally regarded as an effective cap rock unit (Fig. 1c). As a result, the Yuertusi Formation, the Xiaoerbulak Formation, and the Awatag Formation constitute a set of effective source-reservoir-cap assemblages. The Upper Cambrian, consisting of the Xiaqiulitag Formation, developed thick dolomite unit (Fig. 1c). The ISCS currently subdivides the Cambrian Period into four epochs: the Terreneuvian, Epoch 2, Miaolingian, and Furongian (Fig. 1c). The Cambrian chronostratigraphic unit in the eastern Tarim Basin adopts the Kuruktag region “four series and ten stages” stratigraphic subdivision system (Cai et al., 2014), including the Tuershaketag, Mohershan, Xidashan, and Xishanbulak formations (Fig. 1c). The Tuershaketag Group consists of a suite of argillaceous limestone (micritic limestone), corresponding to the Furongian series of the international chronostratigraphy (Fig. 1c). The Miaoling System is composed of the Mohershan Formation, with lithologies mainly dominated by mudstone interbedded with thin limestone (Fig. 1c). The Xishanbulak Formation and the Xidashan Formation constitute the Terreneuvian-Series 2 series of the international chronostratigraphy with lithologies being dominated by a set of mud shale intercalated with siliceous rocks (Fig. 1c). We use this stratigraphic correlation scheme herein in the following description.

Four major ancient continents existed during the Middle–Late Cambrian, including the Gondwana, Siberia, Laurentia, and Baltica (northern Europe) (Golonka, 2009; McKenzie et al., 2011; Lee et al., 2015). The Tarim Basin was a part of the Gondwana supercontinent and was in a low-latitude position similar to South China in the middle Cambrian (Fig. 1b) (Wotte et al., 2007; Wang et al., 2011; Yang et al., 2021a). During the Early–Middle Cambrian, the Gondwana supercontinent near the equator began rapidly drifting southward (Li et al., 2014, 2015). In the Late Cambrian, the Gondwana supercontinent began to drift northward with a slower speed and started to rotate clockwise in the Ordovician (Li et al., 2014, 2015). At the same time, due to glacial ablation, a second-order eustatic sea-level rise occurred during the Cambrian, and the paleocontinents were submerged under shallow water (Miller et al., 2005; Haq and Schutter, 2008). The Middle–Late Cambrian paleoclimate of the Tarim Basin evolved from hot and dry climate to warm and humid climate (Liu et al., 2016; Tian et al., 2018; Fan et al., 2019).

Since the Neoproterozoic, the Tarim and adjacent areas experienced opening, subduction, closure, and accretion in the Paleo-Asian Ocean and the Proto-Tethys Ocean, as well as the collision of micro-continental blocks, which brought multiple tectonism (Xu et al., 2011; Wang et al.,

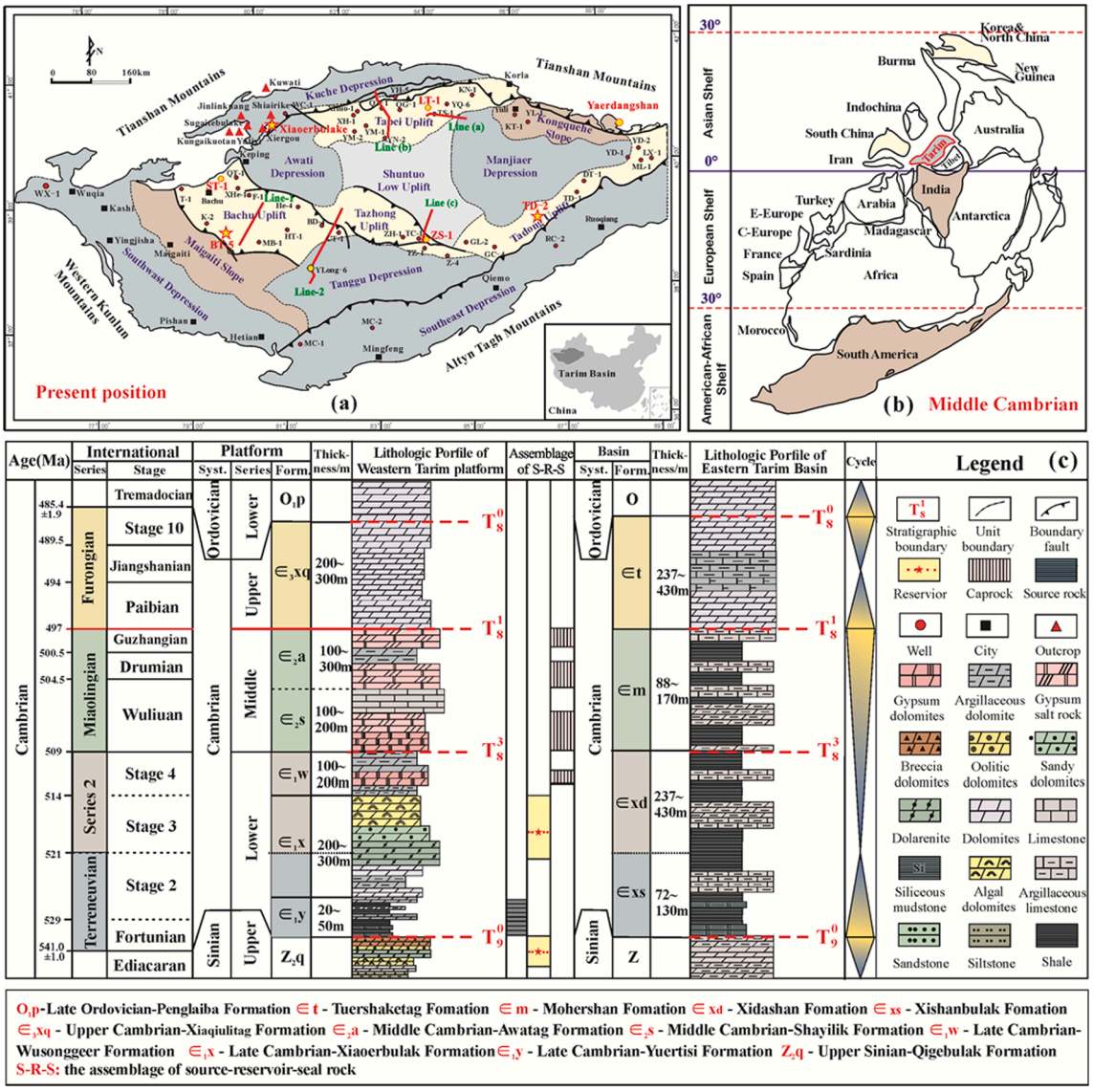

Fig. 1. (a) Map showing the location of the Tarim Basin, NW China and the locations of the Xiaoerbulak outcrop sections in the NW part of the basin and seismic lines investigated; (b) Paleogeography of the Tarim Basin and adjacent continental blocks in the Middle Cambrian (modified from Wang et al., 2017); (c) Generalized stratigraphic section of the Cambrian succession in the Tarim Basin showing stratigraphic subdivision, lithotypes and thickness.

2011). This area saw the development of a series of significant tectonic unconformities extending from the Ediacaran Period up to the Cenozoic era (Lin et al., 2012; Tang, 1994, 1997; Tang et al., 2012). These unconformities, traceable across most of the basin (Fig. 1c), also function as crucial stratigraphic boundaries, such as the Cambrian–Ediacaran boundary (T_9^0), the base of the Middle Cambrian (T_8^3), the base of the Upper Cambrian (T_8^1), and the boundary between the Upper Cambrian and the Ordovician (T_8^0) (Fig. 1c).

3. Materials and methods

3.1. Samples, characterization and analysis

The outcrop section in the Keping area in the northern Tarim Basin, referred to as the Xiaoerbulak (XEBLK) outcrop (Fig. 2), was studied to investigate the boundary between the middle and upper Cambrian (T_8^1). A total of 60 samples were collected across the T_8^1 boundary in the XEBLK outcrop section, all of which were prepared for petrographic characterization. We selected 22 samples that are vein-free, petrographically homogeneous, micritic and fine-grained dolomites for stable carbon and oxygen isotope analyses.

3.2. Geochemical analysis of samples

3.2.1. Carbon and oxygen stable isotope testing method

Geochemical analyses were conducted by the Top-Lab Research Institute of Oil and Gas Development (Beijing). Samples were ground to a size fraction smaller than 200 mesh. They were then dissolved in 100% H_3PO_4 under vacuum and constant-temperature conditions. CO_2 gas was collected for C and O isotope analyses using a MAT-253 isotope ratio mass spectrometer according to the *Standard for Using the Phosphoric Acid Method for Determining C and O Isotope Composition in Carbonate Minerals or Rocks (Z/T0184.17–1997)*. If the sample is limestone, the reaction was set at 25 °C for 24 h. If the sample contains a large amount of dolomite, the reaction was set at 25 °C for 72 h. All isotopic values are reported in delta notation as per mil (‰) in reference to the Pee Dee Belemnite (PDB). The spectrometer has an instrument precision of ± 0.02‰ and an analytical precision of ± 0.15‰ for C isotopes and ± 0.20‰ for O isotopes.

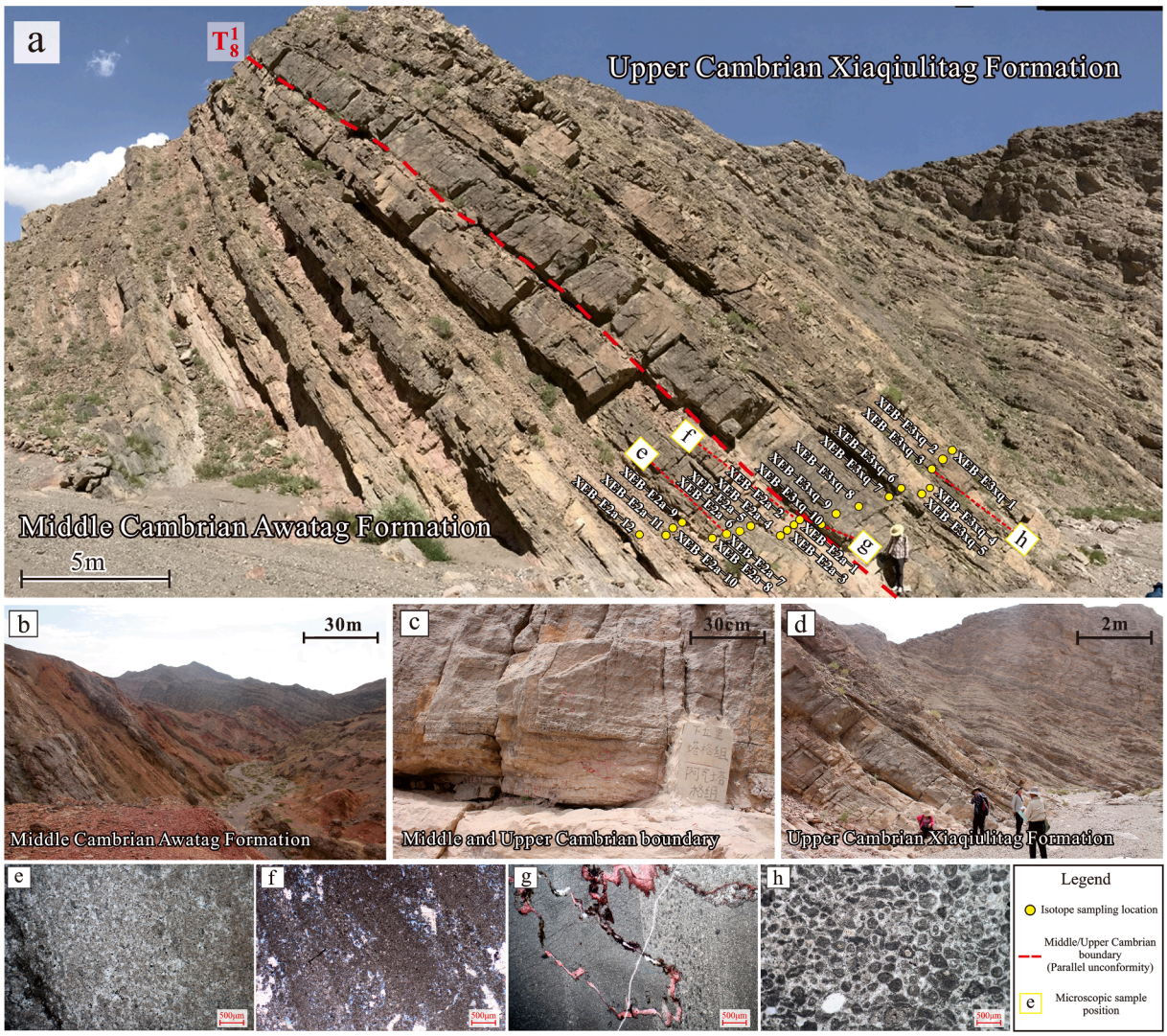

Fig. 2. Field photographs and thin-section photomicrographs of the Xiaoerbulak outcrop section showing the T_8^1 boundary between the Middle Cambrian Awatage Formation and Upper Cambrian Xiaqiulitag Formation (see Fig. 1 for location). The white squares e, f, g, and h on the outcrop mark the positions of thin sections e, f, g, and h. Yellow dots mark the positions of the 22 samples collected for stable isotope analysis. e, finely- powdered crystalline dolomite; f, Stromatolitic dolomite, characterized by Lamellar organic matter bands (Cyanobacterial filaments) with well-developed dissolution pores; g, with a regular erosional interface between dolomicrite and powdered crystalline dolomite; asphalt and calcite fill the cracks. (For interpretation of the references to colour in this figure legend, the reader is referred to the web version of this article.)

3.2.2. *Carbon and oxygen stable isotope data evaluation*

When applying the carbon and oxygen isotopic compositions of carbonate rocks to study the original sedimentary environment, it is usually necessary to assess the degree of diagenetic alteration of the samples. This is because the influence of diagenesis can make it difficult for the $\delta^{13}C$ and $\delta^{18}O$ values of the carbonate rocks to reflect their primary sedimentary characteristics, and instead, they may reflect the characteristics of diagenesis (Allan and Matthews, 1982; Kaufman and Knoll, 1995; Derry, 2010). Therefore, before the use of carbon isotopes for stratigraphic correlation and paleoenvironmental reconstruction, it is necessary to evaluate the reliability of the isotope data.

Carbonate is susceptible to isotopic exchange with meteoric waters and pore fluids in marine sediments during early diagenesis (Allan and Matthews, 1982). It is generally believed that the carbon isotope ratios of carbonate rock samples with $\delta^{18}O$ values between −10‰ and −5‰ may be slightly affected, but such an influence is not sufficient to change their carbon isotope composition. However, if the $\delta^{18}O$ ratio has a high negative value (<-10‰ or −11‰), the original composition of the carbon isotope may have been changed (Derry et al., 1992; Kaufman et al., 1993; Kaufman and Knoll, 1995; Buggisch et al., 2003; Ngia et al., 2019). In addition, the correlation between carbon and oxygen isotopes is also a way to discriminate whether a carbonate sample is affected by diagenetic alteration (Qing and Veizer, 1994; Wang and Feng, 2002). Before using carbon and oxygen isotope data, we used correlation analysis to evaluate the validity of the results.

3.3. *Well data and seismic interpretation data*

This study uses an integrated database that includes an outcrop section, cores from 23 wells, wireline logs of 20 wells, and 2D seismic profiles. All well data and well sample data come from the SINOPEC Northwest Oilfield Branch. A total of 44 2D seismic profiles across the entire basin, processed by SINOPEC Northwest Oilfield Branch and PetroChina Tarim Oilfield Company, were interpreted, providing a firm basis for the recognition of the major unconformity of the Middle and Upper Cambrian boundary. Seismic interpretation was carried out on an HP xw 6600 Workstation using the Landmark 2005 software.

3.4. Method for identifying the boundary between stratigraphic systems

Based on previous studies (Saller, 1994; He et al., 2014; Gao and Fan, 2015; Gao et al., 2016; Wang et al., 2017a), we formulate a comprehensive method for identifying the boundary between stratigraphic systems (or stratigraphic series, or even stratigraphic orders) to avoid the limitations of using a single approach. The method contains the following components: (1) Core and outcrop description; (2) Stable isotope geochemistry correlation; (3) Stratigraphic analysis of seismic data; (4) Well log interpretation; (5) Biostratigraphic analysis of strata below and above unconformities.

4. Boundary identification and geological characteristics

4.1. Identifying the T_8^1 boundary from outcrop

4.1.1. Outcrop location and information

Based on abrupt changes in the sedimentological characteristics between the strata above and below is the most visual and direct method for identifying a boundary (Clari et al., 1995; Miller and West, 1998; Brlek et al., 2014). The Xiaoerbulak section (40°59′19″ N, 80°00′22″ E) is a well-exposed Cambrian outcrop located in the Keping area (see Fig. 1 for its location). This well-exposed section comprises a complete profile from the Cambrian to the Ordovician on the northwestern margin of the Tarim Basin (Yang et al., 2021a; Wu et al., 2021).

4.1.2. Outcrop geological characteristics

In the Xiaoerbulak section, the exposed Upper Cambrian Xiaqiulitag Formation is in parallel unconformable contact with the underlying Middle Cambrian Awatag Formation (Fig. 2a and 2c). The overall lithology of the Awatag Formation consists mainly of light purple-red argillaceous micrite dolomite, gypsum-bearing silt crystal dolomite (Fig. 2e), silt crystalline dolomite, and gypsum mudstone, with minor interbedded sandy dolomite and thin layer gypsum. The lithofacies display distinct cyclical characteristics: the superposition of purple-red argillaceous dolomite and gray-red dolomitic mudstone interbeds (Fig. 2b and 2f), representing a shallowing-upward succession.

The lithology of the Xiaqiulitag Formation is dominated by thick layers of light gray, brown-gray dolomites and grey thickly layered algae dolomite. The formation is characterized by sedimentary structures of microbial origin, a high content of algae, and presence of algal lamina or debris (Fig. 2d and 2h). The lithology across the T_8^1 unconformity consists of gray, thinly-layered dolomite. Dissolution cavities of varying sizes have formed along the bedding below the interface, with local instances of silicification noted (Fig. 2c and 2g).

4.1.3. Analysis of sedimentological characteristics

The boundary between the Upper and the Middle Cambrian (T_8^1) is a second-order sequence boundary, and the lithology changes distinctly across the boundary. The Middle Cambrian Awatag Formation is characteristic of evaporative carbonate platform facies, indicating that the deposition occurred under an arid climate and during a period of sea level fall. The Upper Cambrian Xiaqiulitag Formation is typical of restricted platform facies, indicating an abrupt transition to a deeper water depositional setting above the unconformity relating to sea level rise. The T_8^1 boundary clearly separates two distinct sedimentary settings.

4.2. Identifying the T_8^1 boundary via carbon and oxygen stable isotope data

4.2.1. Carbon and oxygen stable isotope data evaluation

From the Xiaoerbulak section, 22 samples were selected, and all samples have $\delta^{18}O$ values relative to PDB that are heavier than −10‰ (Table 1). In addition, our data show little correlation between $\delta^{13}C_{carb}$ and $\delta^{18}O$ for the entire dataset ($R^2 = 0.0535$) (Fig. 3b), which excludes the possibility of post-depositional fluid alteration (Banner and Hanson, 1990; Jacobsen and Kaufman, 1999).

Table 1
Carbon and Oxygen stable isotopic data from the Upper Cambrian Xiaqiulitag Formation and the Middle Cambrian Awatag Formation at the Xiaoerbulak outcrop section. Sample positions are shown in Fig. 2.

Sample	Formation	Lithology	$\delta^{13}C_{PDB}$‰	$\delta^{18}O_{PDB}$‰	Average value
XEB-E3xq-1	Xiaqiulitag	algal dolomite	−0.3	−7.5	**$\delta^{13}C_{PDB}$‰=-0.5‰**
XEB-E3xq-2	Xiaqiulitag	micrite	−0.8	−7.0	**$\delta^{18}O_{PDB}$‰=-6.64‰**
XEB-E3xq-3	Xiaqiulitag	dolomite	−1.2	−6.1	
XEB-E3xq-4	Xiaqiulitag	algal dolomite	−0.5	−6.7	
XEB-E3xq-5	Xiaqiulitag	algal dolomite	−0.7	−6.5	
XEB-E3xq-6	Xiaqiulitag	dolomite	−0.7	−6.6	
XEB-E3xq-7	Xiaqiulitag	algal dolomite	−0.5	−6.6	
XEB-E3xq-8	Xiaqiulitag	dolomite	0.1	−6.7	
XEB-E3xq-9	Xiaqiulitag	dolomite	0.1	−6.1	
XEB-E3xq-10	Xiaqiulitag	dolomite	−0.2	−5.8	
XEB-E2a-1	Awatag	dolostone	0.5	−6.1	**$\delta^{13}C_{PDB}$‰=0.058‰**
XEB-E2a-2	Awatag	algal dolomite	0.2	−6.3	**$\delta^{18}O_{PDB}$‰=−6.19‰**
XEB-E2a-3	Awatag	algal dolomite	0.3	−6.3	
XEB-E2a-4	Awatag	algal dolomite	0.1	−6.6	
XEB-E2a-5	Awatag	dolomite	0.3	−6.8	
XEB-E2a-6	Awatag	dolomite	0.3	−6.7	
XEB-E2a-7	Awatag	dolomite	0.1	−6.6	
XEB-E2a-8	Awatag	dolomite	−0.9	−5.9	
XEB-E2a-9	Awatag	dolomite	−0.1	−5.5	
XEB-E2a-10	Awatag	dolomite	−0.1	−5.4	
XEB-E2a-11	Awatag	micrite	0.1	−6.1	
XEB-E2a-12	Awatag	dolomite	−0.1	−6.0	

The C and O isotope results (Table 1) can be grouped into three groups based on their stratigraphic locations. The first group, numbered XEB-E2a-1–12, comprises 12 samples from the Middle Cambrian Awatag Formation below the T_8^1 boundary. These samples have $\delta^{13}C$ values of −0.9‰ to 0.5‰ (average: 0.058‰) and $\delta^{18}O$ values of −5.4‰ to −6.8‰ (average: −6.19‰). The second group, numbered XEB-E3xq-1–9, includes 9 samples from the Upper Cambrian Xiaqiulitag Formation, with $\delta^{13}C$ values varying from −1.2‰ to 0.1‰ (average: −0.5‰) and $\delta^{18}O$ values varying from −7.5‰ to −6.1‰ (average: −6.64‰). The third group, numbered XEB-E2a-0, is a single sample from the top of the Middle Cambrian Awatag Formation near the T_8^1 unconformity. The sample has a $\delta^{13}C$ value of −0.2‰ and a $\delta^{18}O$ value of −6.1‰. The $\delta^{13}C$ values range approximately between −1.5‰ and 1.5‰ (Table 1 and Fig. 3), comparable closely to previously published $\delta^{13}C$ values for the Cambrian carbonates globally (Veizer et al., 1999; Wotte and Strauss, 2015).

4.2.2. Analysis of stable carbon and oxygen isotope data

Insights into local environmental changes, like sea-level fluctuations,

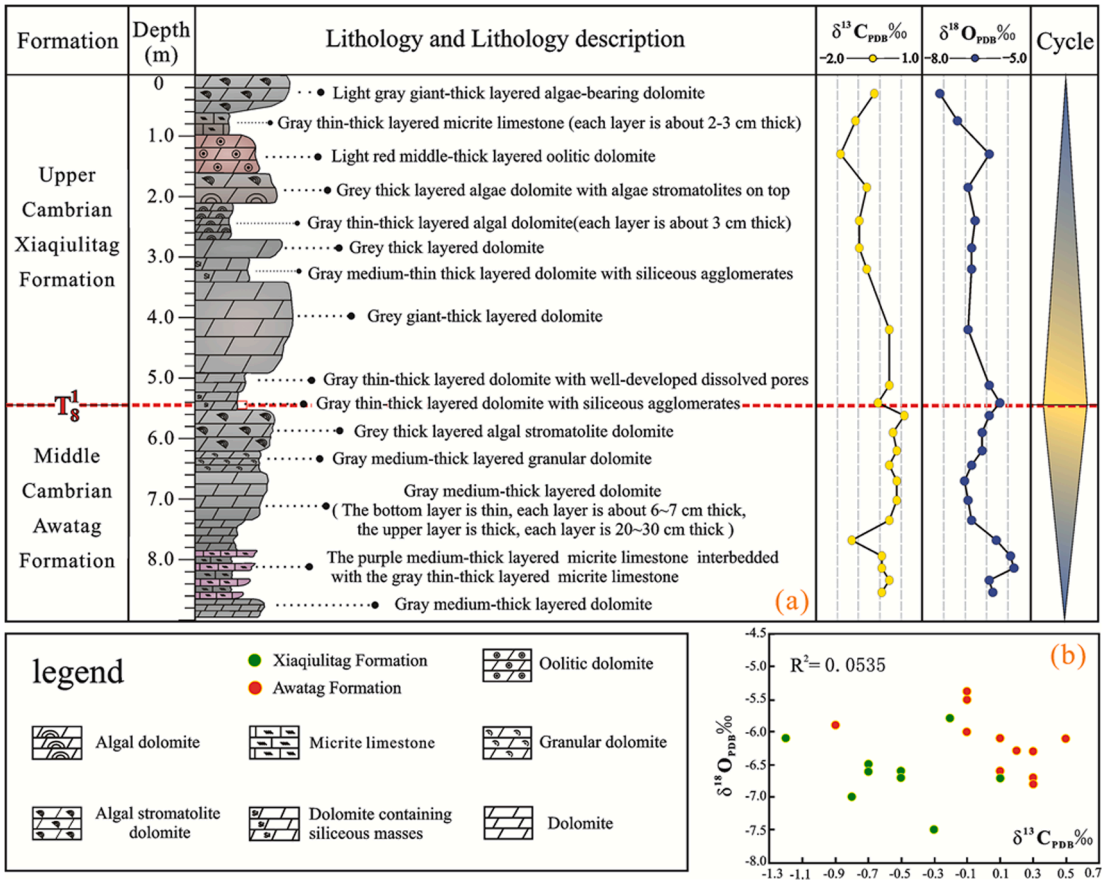

Fig. 3. (a) Characteristics of carbon and oxygen stable isotopes of the middle-upper Cambrian succession at the Xiaoerbulake outcrop in the Tarim Basin (b) Cross plot of $\delta^{13}C$ and $\delta^{18}O$ for samples of the Xiaqiulitag and Awatag formations immediately above and below the T_8^1 boundary.

can be derived from the $\delta^{13}C$ and $\delta^{18}O$ profiles (Miriam and Vincen, 2000; Jiang et al., 2001). Generally, a relatively heavier carbon isotope or lighter oxygen isotope may indicate a local rise in sea level (Zhao, 2015). However, it's important to note that these isotopic variations primarily represent reflect local conditions and are not indicative of global events. Our carbon and oxygen isotope analysis results indicate that both the $\delta^{13}C$ (average: −0.5‰) and $\delta^{18}O$ (average: −6.95‰) ratios above the T_8^1 unconformity are lower than those below the unconformity where the average $\delta^{13}C$ ratio is 0.058‰ and the average $\delta^{18}O$ ratio is −6.19‰ (refer to Table 1 and Fig. 3). This suggests that the sedimentary environments and paleo-water depths of the two formations were different. The Awatag Formation (the Middle Cambrian) was deposited in a strongly oxidizing environment during a period of local sea-level fall under a higher evaporation environment (enriched ^{13}C and heavier $\delta^{18}O$) (Tian et al., 2018; Fan et al., 2019), while the Xiaqiulitag Formation (the Upper Cambrian) was deposited in a reducing environment associated with a local sea-level rise with freshwater input (enriched ^{12}C and lighter $\delta^{18}O$) (Jing et al., 2008; Chen et al., 2015).

Sea level changes, specifically transgression (Guo et al., 2017) or regression (Fanton and Holmden, 2007), can cause negative excursions of carbon isotopes. The oxygen isotopic composition of sea water may be influenced by the input of freshwater (lighter $\delta^{18}O$) or higher evaporation (heavier $\delta^{18}O$). $\delta^{13}C$ and $\delta^{18}O$ excursions are thus useful for identifying any subaerial exposure surfaces in ancient sequences (Allan and Matthews,1982; Ford and Williams, 2007). The C and O isotope results show a negative carbon isotopic excursion (from 0.1‰ to −0.2‰) occurred at the Middle–-Upper Cambrian boundary (Table 1 and Fig. 3) and a positive excursion of the oxygen isotope (from −6.1‰ to −5.8‰) occurred for the same period (Table 1 and Fig. 3). This is because degradation of organic matter in soil can form CO_2, a light C isotope (^{12}C) can be notably enriched in exposed surficial environments during carbonate diagenesis (Allan and Matthews,1982; Li et al., 2000). A negative $\delta^{13}C$ excursion has been recorded at the unconformity interface of the Xiaoerbulak outcrop. The carbonate had been affected by the infiltration of high evaporative water during the exposure, resulting in ^{18}O enrichment at the unconformity interface.

4.3. *Identifying the T_8^1 boundary through wireline logging data*

4.3.1. *Logging curve characteristics*

The Well BT-5 is situated in the Bachu uplift and was drilled down to the Upper Ediacaran strata. The lithology of the Awatag Formation below the boundary is dominated by argillaceous dolomite interbedded with putty crystal dolomite, while the lithology of the Xiaqiulitag Formation above the T_8^1 interface is characterized by crystal powder dolomite interbedded with putty crystal dolomite (Fig. 4). At a depth of 5195 m, the T_8^1 boundary is discernible, with the strata above and below showing parallel unconformable contact (Fig. 4). In the Xiaqiulitag Formation, the gamma-ray (GR), thorium (Th), potassium (K), and uranium (U) log values display no particular patterns, but they peak beneath the T_8^1 unconformity before declining (Fig. 4). Both porosity logs, namely the compensated neutron log (CNL) and the acoustic log (AC), peak near the T_8^1 interface and continue for an interval. The RS and RD average values below the unconformity are lower than that above the unconformity, while the Th/U average values show an opposite pattern.

Well TD-2 is situated in the Eastern Tarim uplift. The strata above and below the boundary present conformable contact (the boundary is at 4778 m) and the argillaceous limestone does not change significantly near the boundary (Fig. 4). According to the natural gamma (GR) and SP

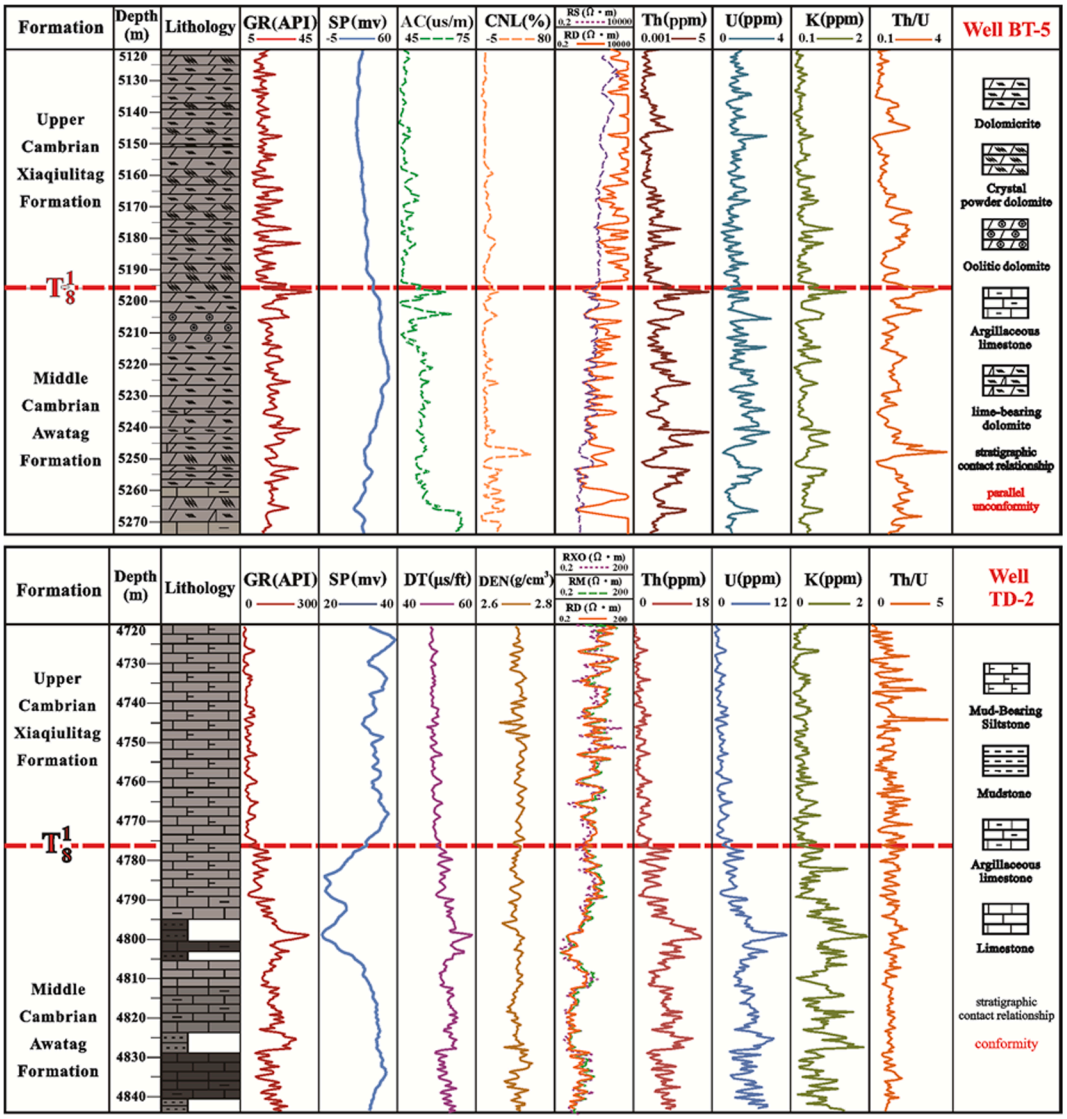

Fig. 4. Petrophysical log characteristics of the Upper Cambrian Xiaqiulitag Formation and the Middle Cambrian Awatag Formation from Well BT-5 on the western Tarim Platform and Well TD-2 in the eastern Tarim Basin (see Fig. 1 for well locations).

logs, it can be seen that the logging facies of the underlying strata have inverse cycle sedimentary characteristics (4778 ~ 4799 m), and the logging facies of the overlying strata have obvious positive cyclical sedimentary characteristics (4745 ~ 4778 m). The CNL, DEN, AC, RS, and RD log values change steadily at the boundary but exhibit different patterns above and below the conformable interface (Fig. 4). The Th, U, K, GR, and DT logs indicate that all average values below the unconformity are considerably higher than those above (Fig. 4).

4.3.2. Analysis of logging data characteristics

With a relatively high vertical resolution and data continuity, logging data can be used to identify boundaries (higher-order sequence boundary) and changes in the vertical sedimentary environment (Gao and Fan, 2015). The GR, Th, U, and K log values can discriminate the argillaceous content in the carbonate rock (positive correlation), thereby providing information on the sedimentary environment and paleo-water depth (Ehrenberg and Svånå, 2001; Gould et al., 2014). Uranium (U) is relatively chemically reactive, and its enrichment mechanism in rocks is primarily due to the reduction and adsorption of U by organic matter during diagenesis (Chen et al., 2004). The concentrations of potassium (K) and thorium (Th) are tied not only to the clay content but also to the alterations in sediment weathering regimes in the source areas (Myers and Bristow, 1989; Jadoon et al., 2016). The thorium to uranium (Th/U) ratio, influenced by sedimentary processes, products, and depositional environment, can be employed to differentiate these environments and processes (Chen et al., 2004; Feng et al., 2016). Because the interface of T_8^1 in Well BT-5 is a parallel unconformity, there were likely regolith formations at the interface, which would be accompanied by the increase of shale content and the enrichment of radioactive substances (Wignall and Twitchett, 1996; Gould et al., 2014). The GR, U, Th, and K logs would thus show abnormally high-value points at the boundary. Simultaneously, in Well BT-5, the data appear to be influenced more by lithological variations, as the GR log profile indicates a substantial change in the proportions of detrital materials. This also accounts for the abrupt shift in Th/U values at this boundary, rather than alterations in the REDOX states of the marine seawater. Brief exposure periods may have led to the erosion of sedimentary strata, thereby amplifying the porosity of residues at the T_8^1 unconformity. Consequently, the CNL and AC logs beneath this interface present segments with unusually high values (Cao et al., 2003). At the T_8^1 boundary of Well TD-2, the strata are in conformable contact, and the logging curves are all in gradual contact without abnormally high values near the boundary. However, the patterns and average values of logs above and below the interface are significantly different, delineating an

interface. For example, the GR and SP logs above and below the interface have different sedimentary rhythm combinations and logging facies combinations (Chen et al., 2004; Li et al., 2007). Therefore, for wells with conformable contacts the boundary may be identified via the changes in logging curve patterns. We can even integrate well logs with seismic data to identify stratigraphy boundaries in areas without drilling data.

4.4. Identifying the T_8^1 boundary via seismic data

4.4.1. Seismic reflection characteristics

The seismic reflection termination types of the T_8^1 unconformity surfaces in the Tarim Basin comprise four categories: (1) synchronous sedimentary (*syn*-sedimentary) exposure unconformities: below the unconformity it displays truncation along the direction of carbonate reef growth, indicating that the platform edges had been subject to exposure (Fig. 5a); (2) overlap unconformities: there is no obvious reflection feature below the seismic sequence boundary, but it displays an onlap relationship above the seismic sequence boundary, representing sedimentary hiatuses (Fig. 5b); (3) tectonic (erosional) unconformities: below the boundary it displays truncation and above the boundary it is characterized by onlap (Fig. 5c); (4) multi-stage (multi-type) superimposed unconformities: multiple seismic sequence boundaries converge into a single reflection as a result of the superposition of the subsequent multi-stage tectonic movement (Fig. 5d).

The seismic facies below the T_8^1 unconformity surface are characterized by high-amplitude and strong continuity reflections. In contrast, the seismic reflectors above the T_8^1 boundary have medium–low amplitude, sometimes even showing disordered-blank reflections, and poor continuity on the seismic profile (Figs. 6 and 7). The architecture and evolution of the platform margin also differ above and below the T_8^1 boundary, from an Early to Middle Cambrian ramp-type carbonate platform to a Late Cambrian rimmed margin-type platform (Fig. 5a). The Early to Middle Cambrian strata in the Tarim Basin developed half-graben structures, graben structures, and fault terrace structures (Fig. 6). These positive faults have a small fault spacing and extend downward to the lower Cambrian bottom boundary below the T_9^0 interface, and upward terminate in the gypsum-salt unit of the Awatag Formation below the T_8^1 interface (Fig. 6).

4.4.2. Analysis of seismic characteristics

Unconformity surfaces can be determined on seismic profiles based on the types of stratal terminations and their lateral correlative surfaces (Lin et al., 2012; Liu et al., 2008). Different seismic reflection termination types usually correspond to unconformities of different origins: truncation clearly represents an angular unconformity, corresponding to denudation and exposure, whereas onlap represents disconformities with minimal erosion corresponding to sedimentary discontinuity (Jacobi and Mitchell, 2002). In addition, seismic facies and seismic features formed by various sedimentary environments can also be used to identify stratigraphic boundaries (Gao et al., 2016). The characteristics of seismic reflection configuration, the exterior shape of the seismic reflection unit, continuity, amplitude, and frequency generally exhibit distinct differences by comparing the seismic features above and below the boundary (Figs. 6 and 7; Liu et al., 2017).

The strata above and below the Upper-middle Cambrian boundary display distinctly different styles of structural characteristics. The interpretation of faults suggests that the Early to Middle Cambrian strata in the Tarim Basin were affected by early Caledonian tectonic movements, leading to the formation of half-graben and graben structures, as

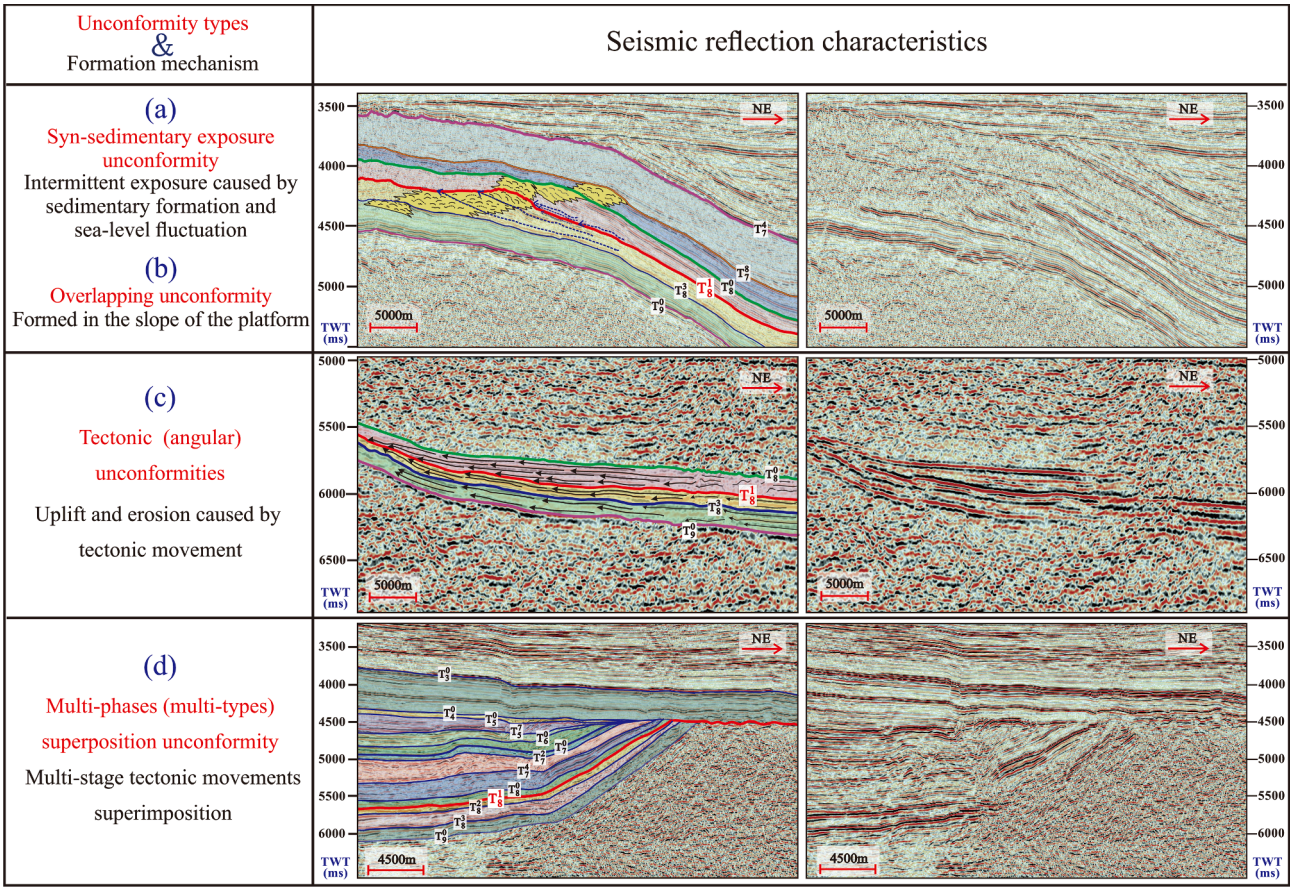

Fig. 5. Varieties of the T_8^1 boundary developed in the study area and characteristics of seismic reflection profiles of the Middle-Upper Cambrian section in the Tarim Basin (Lines a, b, and c; see their locations in Fig. 1).

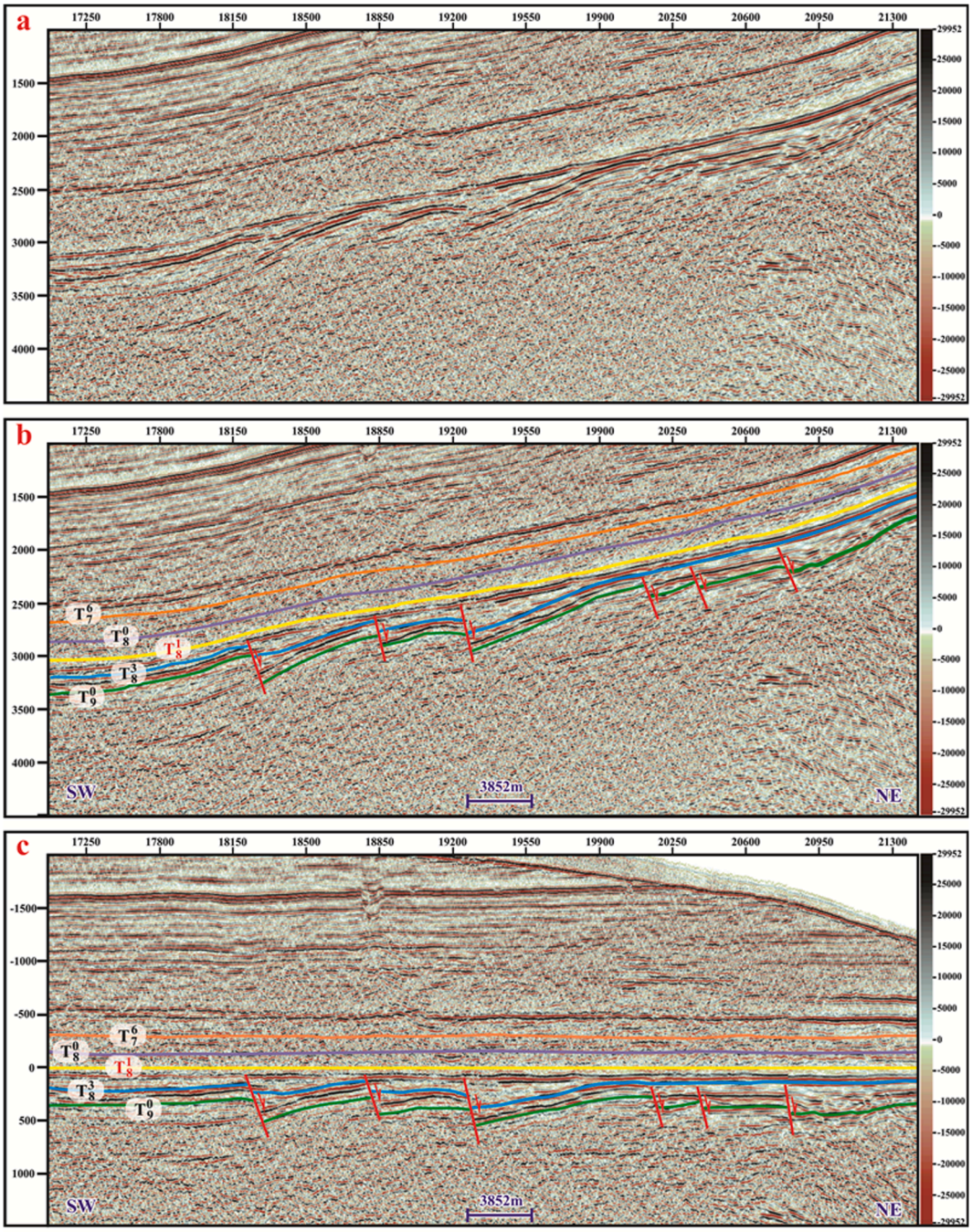

Fig. 6. Seismic reflection profile (Line 1; see its location in Fig. 1) showing the Early-Middle Cambrian half-graben. Line 1 is the seismic profile located at the eastern part of the Bachu Uplift, Tarim Basin (Fig. 1). Asymmetric half-grabens were controlled by major bounding faults. Red line denotes faults, green line marks the base of the Cambrian (T_9^0) boundary, blue line shows the base of the Middle Cambrian (T_8^3), yellow line marks the base of the Late Cambrian (T_8^1) boundary, purple line shows the base of the early Ordovician (T_8^0) boundary. (a-b) Original seismic line, and (c) seismic profile flattened along an originally horizontal surface (base of the Late Cambrian). (For interpretation of the references to colour in this figure legend, the reader is referred to the web version of this article.)

well as fault terraces, under the influence of an extensional tectonic regime (See Fig. 6). The stratal thickness and seismic facies characteristics inside the half-graben show distinct variations, reflecting the sedimentary environment in the half-graben changed (Fig. 6). The fractures had experienced two phases of tectonic movement: In the Early–Middle Cambrian, the extensional motion dominated the development of normal faults and the formation of grabens or half-grabens. In the Late Cambrian, the extension stopped or a brief localized weak compression occurred but it did not change the overall styles of the Early–Middle Cambrian extensional structures (Figs. 6 and 7). This suggests that the fracture systems present above and below the T_8^1 interface evolved under distinct stress regimes.

5. Discussion

5.1. Distribution characteristics of unconformities

By tracing the initial truncated points of the unconformities in seismic profiles across the basin, and comparing sedimentary frameworks and seismic reflection features above and below the T_8^1 boundary with the aid of wireline logging data, the T_8^1 interface is depicted with six manifestations within the Tarim Basin (Fig. 8): a *syn*-sedimentary

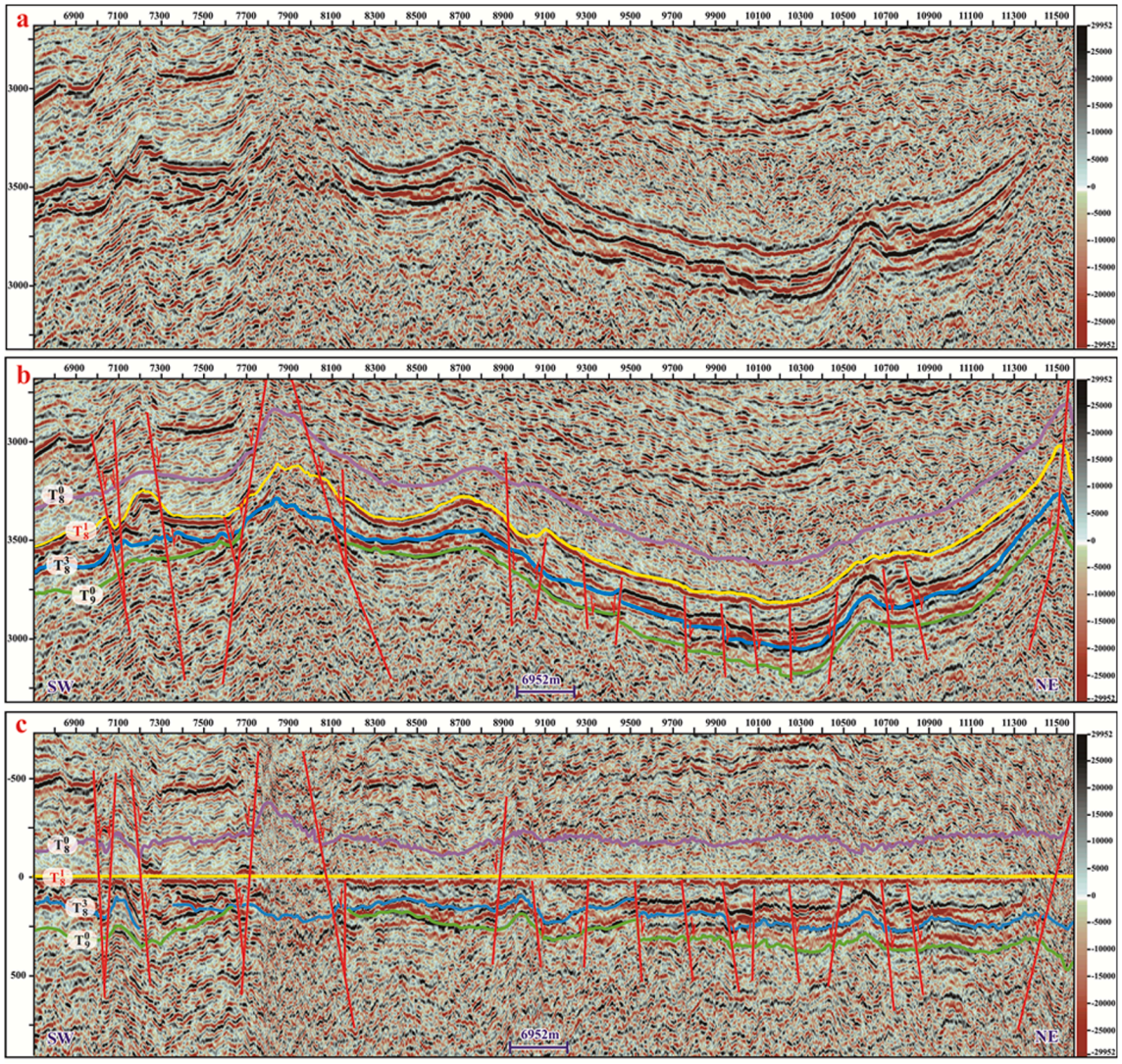

Fig. 7. Seismic reflection profile (Line 2; see Fig. 1 for its location) showing that strata above and below the T_8^1 sequence boundary have distinctively different styles of faulting. Red line denotes faults, green line marks the base of the Cambrian (T_9^0) boundary, blue line shows the base of the Middle Cambrian (T_8^3) boundary, yellow line marks the base of the Late Cambrian (T_8^1) boundary, and purple line shows the base of early Ordovician (T_8^0) boundary. (a-b) Original seismic line, and (c) seismic profile flattened along an originally horizontal surface (base of the Late Cambrian). (For interpretation of the references to colour in this figure legend, the reader is referred to the web version of this article.)

exposure unconformable contact; an overlap unconformable contact; a tectonic erosional unconformable contact; a multi-stage (multi-type) superimposed unconformable contact; a parallel unconformable contact; a conformable contact (Fig. 8). This classification scheme of the stratigraphic contact relationship near the T_8^1 boundary classification scheme is applicable to the entire Cambrian strata in the Tarim Basin.

The *syn*-sedimentary exposure unconformities in the basin are distributed in strips on the edges of two platforms in the Tarim Basin. One is in the northwest, trending NE-SW resembling the shape of a "7". The other is distributed in the eastern part in a "U" shape. Its distinct erosion and truncation characteristics are seen on the top of some platform margin slope belts on the seismic profiles (Fig. 5a-b). Platform types above and below the T_8^1 boundary change upwards from a ramp platform to a rimmed platform setting. The overlap unconformities are characterized by subsequent sedimentary strata forming an onlap contact with the underlying strata, mainly developed in the platform margin slope belt, which is closely related to the distribution and evolution of platform edge in the basin (Fig. 8). As shown in Well TS-1 near the edge of the carbonate platform (Fig. 8), the lithofacies of the strata below the T_8^1 interface comprise interbedded limestone and powder crystal dolomite, indicating that they were deposited in a turbulent water environment, leading to intermittent exposure. The sedimentary facies in this area changed from platform margin mound to platform margin shoal.

The tectonic unconformities (erosional unconformities) with relatively weak denudation are developed extensively in the western part of the platform area (Fig. 8), such as the Magaiti, Yingmaili and Kasa areas. There are obvious truncation features below the boundary and onlap features above the unconformity (Fig. 5c). Certain areas may undergo intense denudation, leading to the removal of strata. For instance, the Middle Cambrian Awatag Formation is entirely absent in Well XHe-1 (Fig. 8).

The multi-stage (multi-type) superimposed unconformities are found in three zones within the Tarim Basin: the northern border of the basin (the Baicheng and Kuche areas), the southern margin (the Tangnan area) and southeast edges of the basin (across the Ruoqiang area) (Fig. 8). From the seismic reflection characteristics, these areas are shown to have experienced multi-stage tectonic movements (Fig. 5d). This is also supported by the data of Well XHuo-1, where the Lower Cambrian strata are in direct contact with the Cretaceous strata with multi-stage

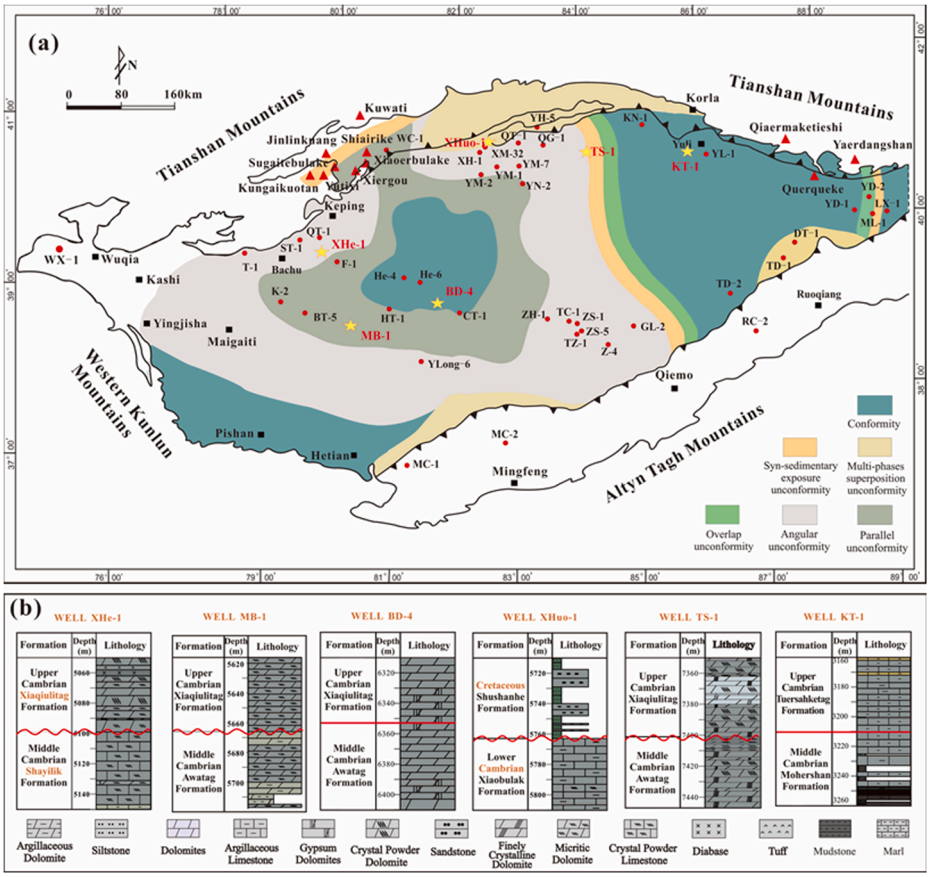

Fig. 8. Types and distribution characteristics of T_8^1 sequence boundary in the Tarim Basin (a) The six manifestations of the T_8^1 boundary and their distribution ranges; (b) Geological features above and below the T_8^1 boundary of the well for each manifestation (the boundary of Well XHe-1 belongs to angular unconformity; the boundaries of Wells BD-4 and KT-1 belong to conformity; the boundary of Well MB-1 belongs to parallel unconformity; the boundary of Well XHuo-1 belongs to multi-phases superposition unconformity; the boundary of Well TS-1 belongs to *syn*-sedimentary exposure unconformity).

unconformities observed between the strata (Fig. 8).

The parallel unconformities are distributed across the central uplift belt in an "O"-shaped pattern, including the Tazhong, Bachu areas and the Keping area of the northwest edge of the basin (Fig. 8). The conformities are distributed in the Awati, Pishan, Hetian areas and the eastern Tarim Basin. In seismic profiles, the Middle Cambrian exhibits strong amplitude and continuous reflection characteristics, while the Upper Cambrian shows chaotic and blank reflection characteristics (see Figs. 6 and 7). The lithology changes near the T_8^1 interface are not obvious (Well MB-1, Well BD-4, and Well KT-1 in Fig. 8).

5.2. *Evolution of the Middle-Upper Cambrian boundary and tectono-sedimentary response analysis*

The types of stratigraphic boundary are mainly controlled by Paleogeomorphic features, tectonic movement, eustacy, and climatic change (Liu et al., 2016). Therefore, the formation process of the interface is often complicated, and the manifestation types of the interface can be traced back to the paleogeomorphic characteristics of the oldest strata and are affected by the evolution process. Based on outcrop and core observation, well-log and seismic data interpretation, combined with tectonic-sedimentary characteristics and the distribution of unconformity types, we divide the Nanhua to the Cambrian (780 Ma-490 Ma) into five stages of evolution to explain the formation process of the T_8^1 boundary.

Stage I:The Nanhua Period (780 Ma-635 Ma) marks the stage of sedimentary evolution from a rift basin to a depressional basin. Rift basins were developed in the Manjiaer Depression including the Southwest Tarim Chasmic and Awati Depression, with a thick layer of clastic sequence (Fig. 9a). The uplift areas formed volcanic highlands due to strong volcanic activity (Fig. 9a). Sedimentation in these rift basins was primarily controlled by normal faults developed in the Nanhua System. At the end of the Nanhua Period, the Kuruktag movement resulted in a major unconformity at the base of the Ediacaran (Zhang and Song, 1998; Wang, 1999; Shi et al., 2018). This stage provided paleotopographic conditions for subsequent sedimentary evolution and the development of the T_8^1 boundary.

Stage II: The Sinian (Ediacaran) Period (635 Ma-541 Ma), characterized by the evolution of the depression. Accompanied by rising sea levels, the depositional area expanded, leading to the formation of three sedimentary systems: the alluvial fan-delta, shore-shelf, and carbonate gentle slope (Fig. 9b). The sedimentary system transitioned from a depressional basin setting to a carbonate platform setting (see Fig. 9b). Operating under a persistent northeast-southwest extension (Yang et al., 2021b), certain normal faults of the Nanhua system developed, exhibiting clear *syn*-depositional characteristics, with growth extending upward to the Ediacaran. Before the deposition of the Cambrian strata, under the influence of the Keping movement, the entire Tarim block was uplifted and subjected to variable denudation, resulting in the development of a major unconformity (T_9^0) between the Ediacaran and Cambrian (Chen et al., 2019b) (Fig. 9c). Synsedimentary normal faults and inherited uplift-depression configurations laid a foundation for the development of the T_8^1 interface.

Stage III: During the deposition of the Early Cambrian Yuertusi Formation, the early Caledonian movement transformed the basin into an extensional state, and an extensive regional transgression occurred (Tian et al., 2020; Pan et al., 2015). Organic-rich shales (high-quality source rocks) were deposited over much of the depression with strata

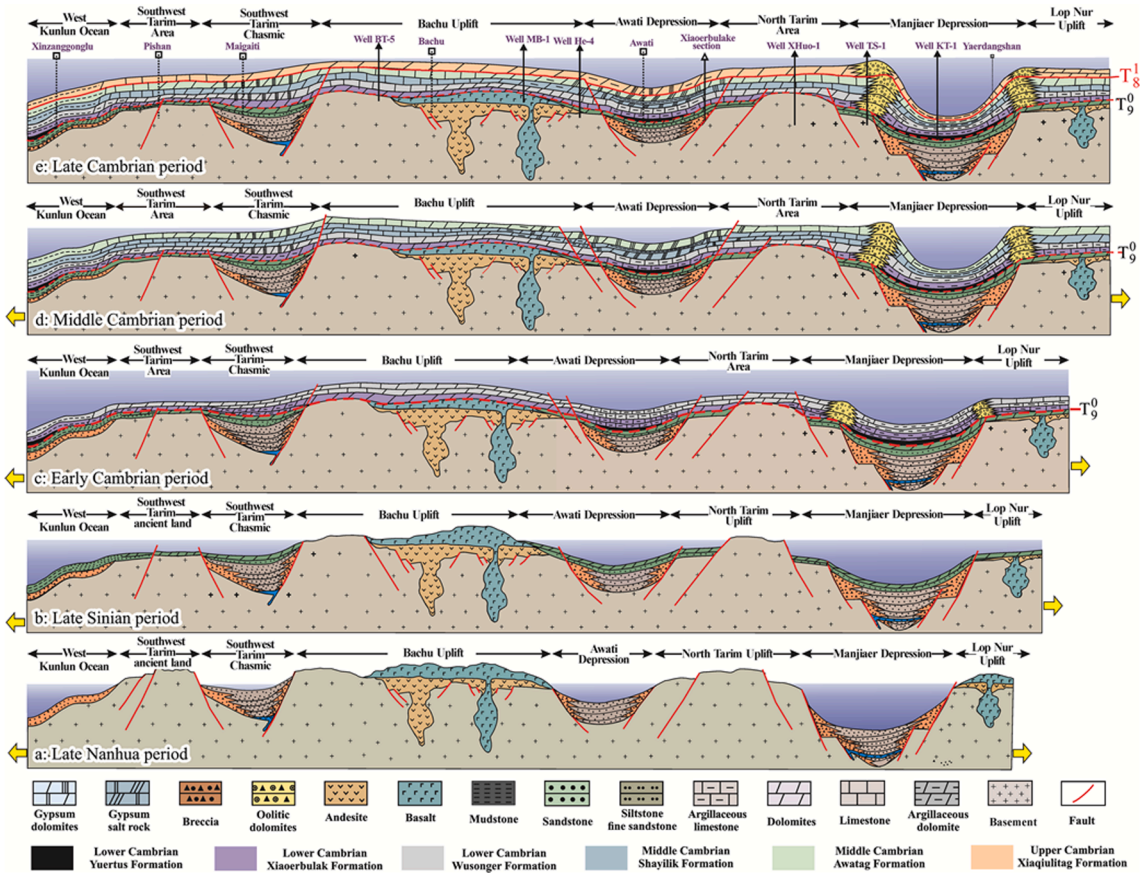

Fig. 9. Sedimentary evolution of the Nanhua-Cambrian successions in the Tarim Basin showing the development process of the T_8^1 sequence boundary (See Fig. 8 for the profile location). The paleotopographic configuration of the basin basement in the Late Nanhua Period (a) is modified from Shi et al., 2018.

thickening in the paleo-valleys and thinning towards platform margins (Fig. 9c). During the deposition of the Xiaoerbulak Formation, as the sea level fell, shallow-water carbonate rocks were developed (Fig. 9c) with broad and gentle-slope dolomitic sand beaches developed on both sides of the Manjiaer rift. Entering the deposition period of the Wusonggeer Formation, the gentle-slope platform sedimentary pattern gradually began to develop into a weakly rimed carbonate platform (Shi et al., 2016) with sea level falling further (Fig. 9c).

Stage IV: During the Middle Cambrian, with continuous sea level fall and platform carbonate growth, sedimentary filling became more prevalent, the paleo-highland disappeared, and the edge of the platform entered into a stage of rapid construction (Fig. 9d; Yang et al., 2021b). The shoulder of the Manjiaer paleo-rift, as a long-term inherited topographic high of the paleo-landform, is the most conducive place for the development of reefal beaches (Fig. 9d; Tian et al., 2020). The rapid catch-up growth of the reef shoals led to the platform edge position prograding seawards (Huang et al., 2020), causing intensive exposure and the development of *syn*-sedimentary unconformity during the regression in the Middle Cambrian Period (Fig. 9d). Because the terrain of the platform margin gradually becomes higher, the reef of platform margin developed a barrier separating the ocean and the platform (Fig. 9d). Due to the high terrain at the platform edge, an overlap unconformity developed at the slope of the platform. Under a backdrop of a mild extensional structure, a few normal faults evolved within the Nanhua System, possibly through inheritance (Fig. 9d). These faults shaped the configuration of the Tarim Basin, leading to the formation of depressions in the Manjiaer and Shuntuogule regions, as well as faulted depressions in the Bachu and Tazhong areas. This established a paleotopographic regime, fostering the development of an evaporative lagoon within the platform (see Fig. 9d). Normal faults with roughly the same occurrence were developed around the evaporative lagoon, forming step-like composite faults (Figs. 6 and 7) and leading to the development of a structural/erosional unconformity between the Middle and Late Cambrian. The hot and dry paleo-climate of the Middle Cambrian resulted in a closed evaporative environment in the intra-platform depression (lagoon), where thick gypsum salt rocks were deposited, forming effective caprocks (Fig. 9d). Due to the low topography of the intra-platform depression, the enclosed water body is quite stagnant, the hydrodynamic force is weak, there is no strong tectonic activity but continuous deposition, the Middle and the Upper Cambrian are thus in a conformable contact (Fig. 9d). As the peripheral areas of the Tarim Basin have experienced multiple periods of tectonic movement, strong subsequent erosion may have eroded the underlying strata and formed unconformities (Fig. 9d). Multiple unconformities were thus superimposed over different periods, forming superimposed unconformities (Fig. 9d).

Stage V: The Late Cambrian Period marks a stage of open platform construction, during which brief large-scale transgression occurred, the reef-building at the edge of the platform became weakened, while the growth position of reefs migrated into the platform (Fig. 9e). On the seismic profile, the early Caledonian normal faults do not cut across the middle Cambrian, indicating the disappearance of a weakly extensional or a passive continental margin environment (Figs. 6, 7, and 9e). This conclusion contradicts the view that the Tarim block was in a strong stretching stage during the Cambrian Period as recognized by previous researchers (Zhu et al., 2019b) (Fig. 9e).

The distribution and types of unconformities reflect the nature of the depositional-erosional processes and sea-level fluctuations. In the Tarim Basin, the boundary between the Middle and Upper Cambrian, particularly the area associated with conformable contact, can represent

lagoonal facies deposition, as exemplified by the deposition of Middle Cambrian gypsum salt on the platform. Moreover, the Yuertus Formation of the Lower Cambrian in the Tarim Basin exhibits well-developed source rocks. Synchronous sedimentary exposure unconformity in the Middle Cambrian would represent areas dominated by platform marginal facies deposits, typical of high-quality reservoirs. Tectonic (erosional) unconformity indicates the occurrence of tectonic movement and is often associated with fractures caused by tectonic movement. In case the tectonic (erosional) unconformity occurs in the gypsum flat sedimentary facies, it may develop an exposed environment near the interface, thereby developing gypsum flat dolomite reservoirs. The manifestation of the boundary can thus reflect the regional tectonic changes in the peripheral areas of the Tarim Basin and the sedimentary changes within the basin. It may also be indicative of the development of a source-reservoir-cap assemblage within the Tarim Basin.

5.3. Global correlation of carbon isotope signatures of the Middle-Upper Cambrian boundary and causes for the absence of the SPICE event in western Tarim Basin

The stratigraphic subdivision and correlation of the Cambrian chronostratigraphy in the Tarim Basin is an issue that has not yet been resolved because two distinctly different stratigraphic subdivision schemes have been respectively used in the western and eastern parts of the basin and the traditional "Middle Cambrian" and "Late Cambrian" in the Tarim Basin cannot be directly correlated with the "Miaolingian" and "Furongian". At the same time, due to the lack of mega-fossil markers in the Cambrian strata of the Tarim Basin, it is difficult to establish isochronous stratigraphic correlation via the biostratigraphic methods. Large-scale carbon-isotope excursions, which can be directly correlated to global paleo-climate, evolutionary events, sea-level fluctuations, etc. are often found to coincide with chronostratigraphic boundaries (Li et al., 2017b; Wang et al., 2017b; Babcock et al., 2015) (Fig. 10). Therefore, Cambrian carbon isotopic excursions in the Tarim Basin offers an indispensable technique to subdivide and correlate the middle-upper Cambrian boundary.

Four major excursions have been identified during the Middle-Late Cambrian Period (Fig. 10), including three negative $\delta^{13}C$ excursions (TOCE, DICE, and ROECE) and one distinct positive $\delta^{13}C$ excursion (SPICE). The Lower/Middle Cambrian boundary (base of the Shayilik Formation) in the Tarim Basin can be correlated to the international Miaolingian/Series 2 boundary by using the Redlichiid Olenellid Extinction Carbon Isotope Excursion (ROECE) as an important isochronous correlation marker (Jing et al., 2008; Wang et al., 2011; Guo et al., 2017). The Drumian Carbon Isotope Excursion (DICE) is an important marker for the global correlation for the lower boundary of the Drumian stage (Yang et al., 2021a). It may be isochronously correlated to the Awatage Formation in the western Tarim Platform and the lower part of the Mohershan Formation (Chen et al., 2019a). The SPICE event is generally recorded in the Upper Cambrian (the Furong Series) sedimentary strata of almost every paleo-continent, such as South China Block (Zuo et al., 2018; Zhu et al., 2004), North China Block (Zuo et al., 2020), Kazakhstan (Saltzman et al., 2000 and 2004), Siberia (Kouchinsky et al., 2008), North America (Saltzman et al., 1998; Montañez et al., 2000), etc. The SPICE event is also recorded in the eastern Tarim Basin (Wang et al., 2020b; Liu et al., 2017), but there is still a scant record of the SPICE event in the western part of the Tarim Basin. Therefore, there are some difficulties in determining the boundary of the Middle–Upper Cambrian and establishing an isochronous correlation framework for the Miaolingian series to the Furongian series.

Veizer et al. (1999) showed that these large positive or negative carbon-isotope excursions represent stratigraphic boundaries. By analyzing the carbon isotope data of the Xiaoerbrake type section in the Keping area, the LT-1, ST-1, and ZS-1 wells in the western Tarim area, the Yaerdangshan section and Well Tadong-2 in the eastern Tarim area (Fig. 11), we have found that all the $\delta^{13}C$ enrichment anomalies during the Cambrian are corresponding to the established general trend of sea level change. Based on carbon isotope data, we first establish the

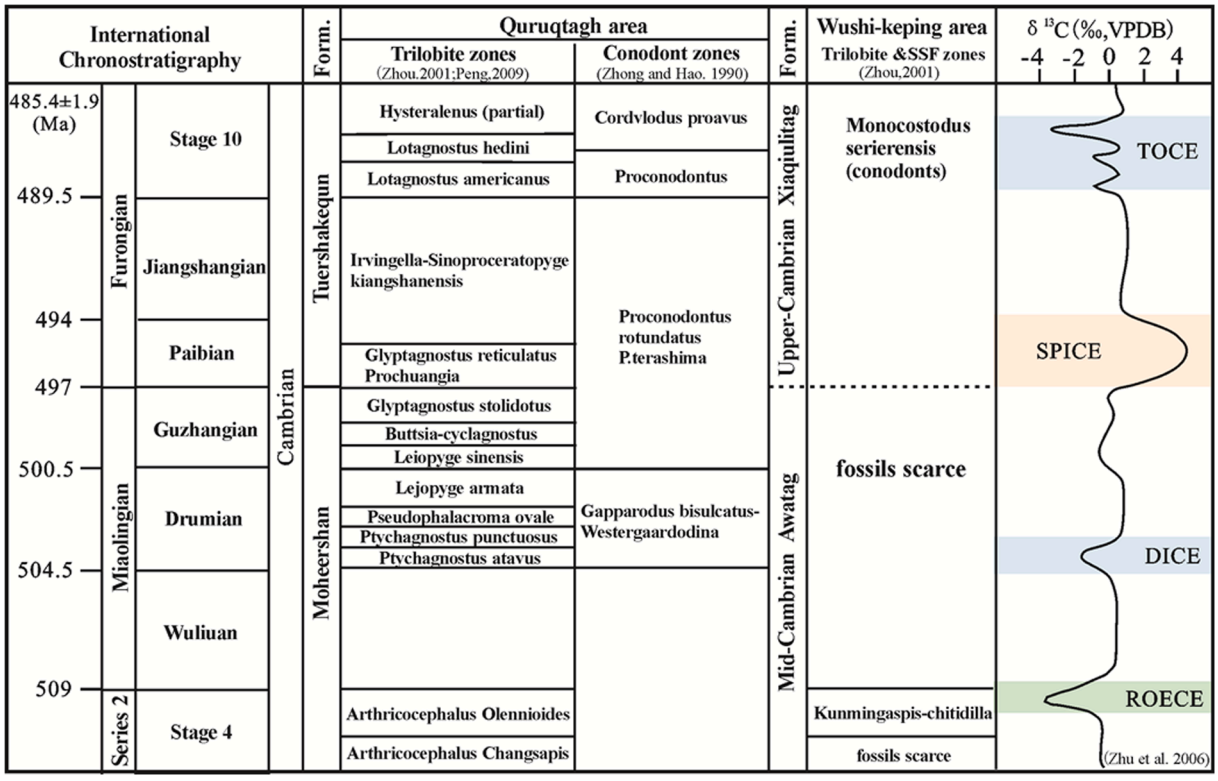

Fig.10. Biostratigraphic correlation of the Wushi-Keping area (western Tarim Basin) and Quruqtagh area (eastern Tarim) (Zhou, 2001; Peng, 2009; Zhong and Hao, 1990). The $\delta^{13}C$ data and Cambrian evolutionary events are modified after Zhu et al., 2006.

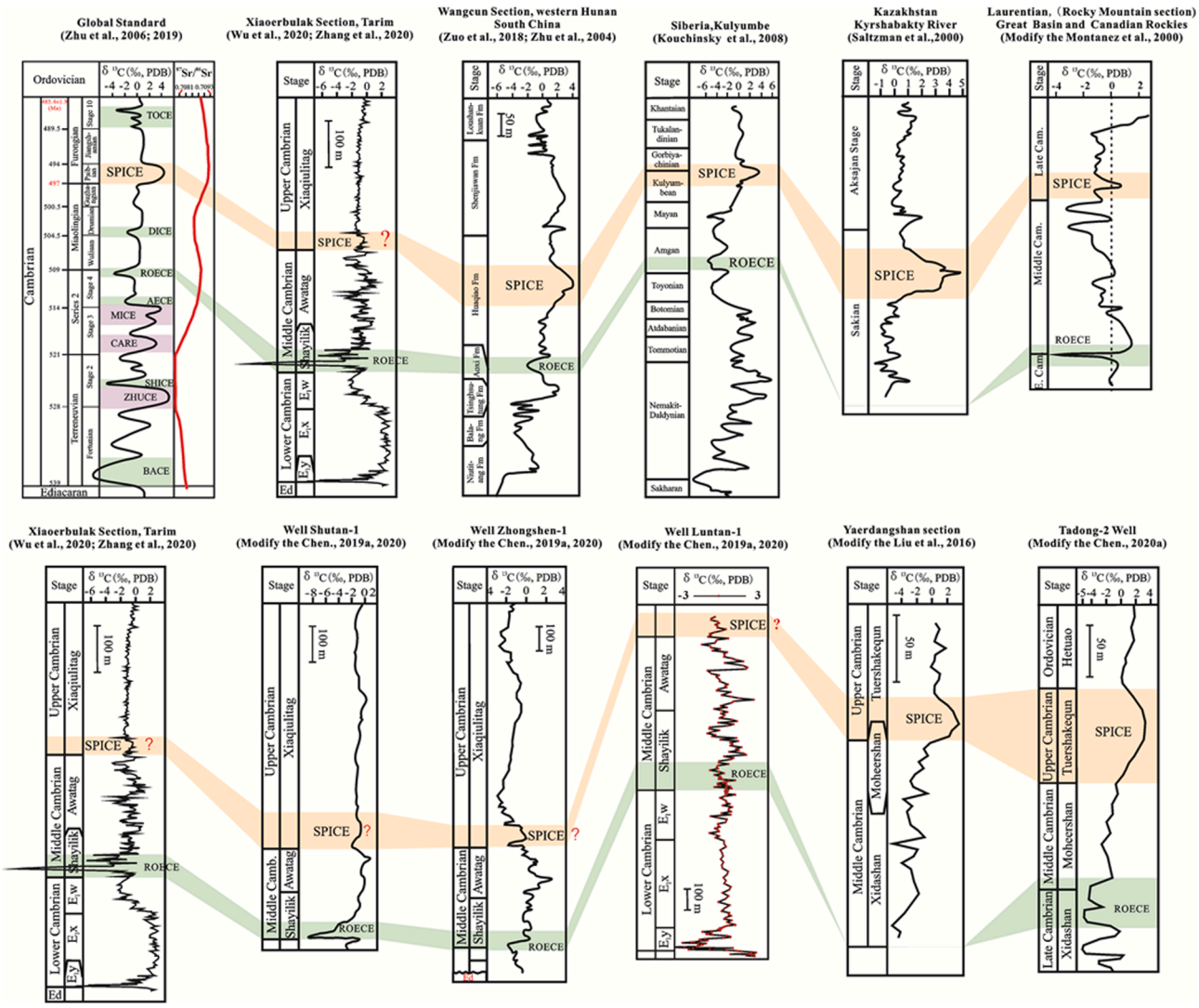

Fig. 11. Cross correlation of SPICE event within the global chronostratigraphic framework and the Middle-Upper Cambrian carbon isotope chemostratigraphy in the Tarim Basin.

position of the ROECE event corresponding to the boundary between the Middle and Lower Cambrian. At the T_8^1 interface (the boundary of the Middle/Upper Cambrian), the value of $\delta^{13}C$ exhibits a larger negative excursion (Fig. 11). The data show that all the initial $\delta^{13}C$ values are about $0 \pm 1‰$, the peak $\delta^{13}C$ values are $-1‰$ to $-2‰$, and the average excursion amplitude is about 1‰ (Figs. 3 and 11). There are also distinct differences in the characteristics of the $\delta^{13}C$ signatures across the boundary: The $\delta^{13}C$ values change above the boundary is relatively gentle with weak volatility, whereas the $\delta^{13}C$ values below the boundary have a large change and strong fluctuations (Fig. 11). It is thus concluded that the base of the Xiaqiulitag Formation in the western part of the Tarim Basin may correspond to the base of the Tuershaketag Formation in the eastern part of the Tarim Basin.

A worldwide mass extinction of trilobites at the base of the *Glyptagnostus reticulatus* Biozone marks the beginning of the SPICE excursion (Saltzman et al. 2000) (Fig. 10). Researchers have previously found that characteristic trilobites of the Furongian appear at the base of the Tuershaketag Formation in the Quruqtagh area in the eastern part of the Tarim Basin (Zhang, 1985; Zhou and Hao, 1990; Zhou and Chen, 1990; Zhou, 2001). Therefore, it can be reasonably confirmed that the base of the Tuershaketag Formation is the base of the Furongian (Fig. 10) and the SPICE event may be present within the Xiaqiulitag Formation and Tuershaketag Formation (Fig. 10). The $\delta^{13}C$ curves from the Yaerdang profile and Tadong-2 core samples record the SPICE event (Fig. 11), implying that the two profiles are comparable. The SPICE event above the Middle-Upper Cambrian boundary is characterized by a distinct positive excursion of carbon isotope (Fig. 11). However, the SPICE event is rarely reported in the western part of the Tarim Basin.

It is not clear whether the absence of the SPICE event was caused by a depositional hiatus nearby the T_8^1 boundary or our investigation and sampling are insufficient. Here, we propose that the weak negative excursion before the sharply positive excursion of carbon isotope as an isotopic stratigraphic marker for determining the Middle/Upper Cambrian boundary in the Tarim Basin, which should correspond to the boundary between the Furongian and the Miaolingian. We further consider that the developmental unconformity of the T_8^1 boundary had somehow caused the absence of the SPICE event in the western part of the Tarim Basin. The Xiaoerbrake section, the LT-1, ST-1 and ZS-1 wells are all located in areas associated with parallel unconformity or angular unconformity in the western Tarim Basin (Fig. 11). These areas have experienced depositional hiatus, thus the SPICE event would not be recorded in these $\delta^{13}C$ curves. This also lead to the lack of biomarkers at the bottom of the Furongian (Fig. 11). However, the Yaerdangshan outcrop section and Well Tadong-2 are located in an area of conformable contact at the T_8^1 interface in the western Tarim Basin that did not experience depositional hiatus (Fig. 11). The base of the Tuershaketag

Formation (above T_8^1 boundary) recorded the *Glyptagnostus reticulatus* Biozone markers of the Furongian (Fig. 10). Additionally, the carbon isotope data from this outcrop also records the SPICE event (Fig. 11).

The absence of the SPICE event and the development of unconformity are also reported for the Laurentia and Gondwana paleocontinents, similar to the western Tarim Basin scenario: In the Laurentia paleocontinents, such as northwestern Wyoming and northern Vermont, the Cambrian Miaolingian–Furongian boundary is characterized by an unconformity (the carbonate platform experiences local subaerial exposure) leading to the absence of the SPICE excursion locally and the missing the trilobite biozones including the Dunderbergia Zone (Palmer, 1981; Chow and James, 1987; Saltzman et al., 1998, 2004; Glumac and Spivak-Birndorf, 2002; Morgan, 2013). In the Gondwana paleocontinent, studies from the western Mediterranean region (e.g., Morocco, Spain, and France) (Álvaro et al., 2007), the Sino-Korean Block (Chen et al., 2011), Iran (Bayet-Goll et al., 2014; Geyer et al., 2014) have also recorded widespread occurrences of unconformities accompanied by a relative sea-level fall followed by a global transgression (Crossley and McDougall, 1998; Park and Choi, 2011; Park et al., 2013). The absence of the SPICE event in the western Tarim Basin is thus not a special case, and it is likely caused by depositional hiatus recorded as the T_8^1 interface.

6. Conclusions

(1) The boundary between the Middle and the Upper Cambrian, T_8^1, in the Tarim Basin, western China, has been identified based on distinct changes of sedimentary facies, stable carbon and oxygen chemostratigraphy, seismic and well log signatures below and above the boundary.

(2) The T_8^1 boundary across the Tarim Basin has six manifestations, which are controlled by a combination of various factors including paleogeomorphology, tectonic movement, eustacy and climatic change: (i) The *syn*-sedimentary unconformities are distributed in strips extending from the northeast to the southwest around the basin edges, due to continuous sea level fall and a rapid growth/buildup of carbonate reef shoals; (ii) The overlap unconformities were developed by the upper Cambrian sedimentary strata overlapping the slope of the carbonate platform, as a result of the high terrain at the platform edge; (iii) The multistage (multi-type) superimposed unconformities are confined to the basin edges, controlled mainly by multi-stage tectonic movements; (iv) The tectonic unconformities (erosion unconformities) are distributed across the central uplift belt in an "O"-shaped pattern with a complex formation mechanism jointly controlled by faults formed in the Nanhua system, sea level fall, and paleotopography; (v) The parallel unconformities are developed in the western platform and the Keping areas, relating to sea level falls and existing paleotopography; and (vi) The conformities developed corresponding to areas where lagoons developed, being controlled mainly by paleotopography inherited from the Nanhua Period. The T_8^1 boundary within the Tarim Basin appears to manifest a good coupled tectonic-sedimentary effect. Areas of conformity can be used as a proxy for lagoon facies, dominated by gypsum-salt rocks; areas of synchronous sedimentary unconformities are usually associated with platform marginal facies that are typical of high-quality reservoirs; while areas associated with tectonic erosional unconformity are prone to develop fractures due to tectonic movement.

(3) The $\delta^{13}C$ weak negative excursion before a sharp positive excursion in the Middle/Upper Cambrian is proposed here as an isotopic stratigraphic marker for the T_8^1 boundary. The boundary between the Awatag and Xiaqiulitag formations on the western Tarim Platform should thus align with the boundary between the Tuershaketag and Mohershan formations in the eastern Tarim Basin, as well as the boundary between the Furongian and Miaolingian. The absence of the SPICE event in the western part of the Tarim Basin may be due to stratal hiatus as a result of the development of an unconformity associated with the T_8^1 boundary.

CRediT authorship contribution statement

Yaxin Shang: Conceptualization, Methodology, Investigation, Writing – original draft. **Keyu Liu:** Conceptualization, Writing – review & editing, Validation. **Zhiqian Gao:** Methodology, Supervision, Project administration, Funding acquisition, Resources. **Chenjia Zhang:** Data curation, Investigation. **Ziyi Wang:** Data curation, Investigation.

Declaration of Competing Interest

The authors declare that they have no known competing financial interests or personal relationships that could have appeared to influence the work reported in this paper.

Data availability

Data will be made available on request.

Acknowledgments

This work is supported by the National Natural Science Foundation of China (Grants 41972130, U19B6003-01-02). We sincerely thank SINOPEC Northwest Oilfield Branch and PetroChina Tarim Oilfield Company for providing well log and seismic data. Special appreciation is expressed to Editor-in-Chief Zhou who helped with editing the manuscript. We thank two anonymous reviewers for their thorough and critical reviews and suggestions, which greatly improved the manuscript.

References

Ahlberg, P., Axheimer, N., Babcock, L.E., Eriksson, M.E., Schmitz, B., Terfelt, F., 2010. Cambrian high-resolution biostratigraphy and carbon isotope chemostratigraphy in Scania, Sweden: first record of the SPICE and DICE excursions in Scandinavia. Lethaia 42 (1), 2–16.

Allan, J.R., Matthews, R.K., 1982. Isotope signatures associated with early meteoric diagenesis. Sedimentology 29 (6), 797–817.

Álvaro, J.J., Ferretti, A., González-Gómez, C., Serpagli, E., Tortello, M.F., Vecoli, M., Vizcaïno, D., 2007. A review of the Late Cambrian (Furongian) palaeogeography in the western Mediterranean region, NW Gondwana. Earth Sci. Rev. 85 (1–2), 47–81.

Babcock, L.E., Peng, S., Geyer, G., Shergold, J.H., 2005. Changing perspectives on Cambrian chronostratigraphy and progress toward subdivision of the Cambrian System. Geosci. J. 9 (2), 101–106.

Babcock, L.E., Peng, S.C., Brett, C.E., Zhu, M.Y., Ahlberg, P., Bevis, M., Robison, R.A., 2015. Global climate, sea level cycles, and biotic events in the Cambrian Period. Palaeoworld 24 (1–2), 5–15.

Banner, J.L., Hanson, G.N., 1990. Calculation of simultaneous isotopic and trace element variations during water-rock interaction with applications to carbonate diagenesis. Geochim. Cosmochim. Acta 54 (11), 3123–3137.

Bayet-Goll, A., Geyer, G., Wilmsen, M., Mahboubi, A., Moussavi-Harami, R., 2014. Facies architecture, depositional environments, and sequence stratigraphy of the Middle Cambrian Fasham and Deh-Sufiyan Formations in the central Alborz, Iran. Facies 60 (3), 815–841.

Brlek, M., Korbar, T., Košir, A., Glumac, B., Grizelj, A., Otoničar, B., 2014. Discontinuity surfaces in Upper Cretaceous to Paleogene carbonates of central Dalmatia (Croatia): Glossifungites ichnofacies, biogenic calcretes, and stratigraphic implications. Facies 60 (2), 467–487.

Buggisch, W., Keller, M., Lehnert, O., 2003. Carbon isotope record of Late Cambrian to Early Ordovician carbonates of the Argentine Precordillera. Palaeogeogr. Palaeoclimatol. Palaeoecol. 195 (3–4), 357–373.

Cai, X.Y., Dou, L.W., Cai, H.S., Yu, T.X., Cao, Z.C., 2014. Classification and correlation of Cambrian in eastern Tarim Basin. Pet. Geol. Exp. 36 (5), 539–545.

Cao, Y.C., Jiang, Z.X., Xia, B., Wang, J.F., Yang, W.L., Wang, W.H., 2003. Some methods for identifying sequence boundaries and condensation sections using well logging. J. Petrol. Sci. 27 (2), 23–26.

Carter, R.M., Fulthorpe, C.S., Naish, T.R., 1998. Sequence concepts at seismic and outcrop scale: the distinction between physical and conceptual stratigraphic surfaces. Sed. Geol. 122 (1), 165–179.

Chen, Z.H., Cha, M., Jin, Q., 2004. Application of natural gamma ray logging and natural gamma spectrometry logging to recovering paleoenvironment of sedimentary basin. Chinese J. Geophys. (in Chinese) 47 (6), 1145–1150.
Chen, J.T., Chough, S.K., Han, Z.Z., Lee, J.H., 2011. An extensive erosion surface of a strongly deformed limestone bed in the Gushan and Chaomidian formations (late Middle Cambrian to Furongian), Shandong Province, China: Sequence–stratigraphic implications. Sed. Geol. 233 (1–4), 129–149.
Chen, J.T., Chough, S.K., Lee, J.H., Han, Z.Z., 2012. Sequence-stratigraphic comparison of the upper Cambrian Series 3 to Furongian succession between the Shandong region, China and the Taebaek area, Korea: high variability of bounding surfaces in an epeiric platform. Geosci. J. 16 (4), 357–379.
Chen, Y.Q., Yan, W., Han, C.W., Yan, L., Ran, Q.G., Kang, Q., He, H., Ma, Y., 2019b. Structural and sedimentary basin transformation at the Cambrian/Neoproterozoic interval in Tarim Basin: Implication to subsalt dolostone exploration, 30(1), 39-50.
Chen, Y.Q., Yan, W., Han, C.W., Yang, P.F., Li, Z., 2015. Redefinition on structural paleogeography and lithofacies paleogeography framework from Cambrian to Early Ordovician in the Tarim Basin: A new approach based on seismic stratigraphy evidence. Nat. Gas Geosci. 26 (10), 1831–1843.
Chen, Y.Q., Zhang, Y.Q., Zhou, P., Kaderer, A., 2019b. Carbon isotope stratigraphy and correlation of the Cambrian Miaolingian Strata, Tarim Basin. J. Stratigr. 43, 324–332.
Chen, Y.Q., Huang, J.H., Yang, P.F., Yi, Y., Yang, G., 2020b. Carbon isotope chemostratigraphy and time frame of Cambrian in western platform. Tarim Basin. Geological Review 66 (1), 59–71.
Chow, N., James, N.P., 1987. Cambrian grand cycles: a northern Appalachian perspective. Geol. Soc. Am. Bull. 98 (4), 418–429.
Clari, P.A., Pierre, F.D., Martire, L., 1995. Discontinuities in carbonate successions: identification, interpretation and classification of some Italian examples. Sed. Geol. 100 (1–4), 97–121.
Crossley, R., McDougall, N., 1998. Lower palaeozoic reservoirs of North Africa. In: MacGregor, D.S., Moddy, R.T.J., Clark Lowes, D.D. (Eds.), Petroleum Geology of North Africa. Geological Society of London Special Publication 132. Geological Society of London, 132(1), 157-166.
Darroch, S.A., Smith, E.F., Laflamme, M., Erwin, D.H., 2018. Ediacaran Extinction and Cambrian Explosion. Trends Ecol. Evol. 33 (9), 653–663.
Derry, L.A., 2010. A burial diagenesis origin for the Ediacaran Shuram-Wonoka carbon isotope anomaly. Earth Planet. Sci. Lett. 294 (1–2), 152–162.
Derry, L.A., Kaufman, A.J., Jacobsen, S.B., 1992. Sedimentary cycling and environmental change in the Late Proterozoic: evidence from stable and radiogenic isotopes. Geochim. Cosmochim. Acta 56 (3), 1317–1329.
Ehrenberg, S.N., Svånå, T.A., 2001. Use of spectral gamma-ray signature to interpret stratigraphic surfaces in carbonate strata: An example from the Finnmark carbonate platform (Carboniferous-Permian), Barents Sea. AAPG Bull. 85 (2), 295–308.
Fan, Q.Q., Lu, S.F., Li, H., Pan, W.Q., Zhang, B.S., Zhang, Y.Y., Tan, Z.Z., 2019. Geochemical characteristics and geological significance for petroleum of the Middle-Lower Cambrian marine strata: A case study of Keping area in the Tarim basin. J. China Univ. Min. Technol. 48 (2), 377–394.
Fanton, K.C., Holmden, F.C., 2007. Sea-level forcing of carbon isotope excursions in epeiric seas: implications for chemostratigraphy. Can. J. Earth Sci. 44 (6), 807–818.
Feng, W.M., Xie, Y., Liu, J.G., Lin, J.S., Chen, G., Zhao, Z., 2016. Sedimentological significance of natural gamma ray logging data of marine carbonate: a case of the well L1 of Qingxudong formation, lower cambrian in Southeast Sichuan Basin. Mar. Geol. Quat. Geol. 36 (5), 165–172.
Ford, D.C., Williams, P.W., 2007. Karst hydrogeology and geomorphology, Vol. 576. John Wiley & Sons, Chichester.
Gao, Z.Q., Fan, T.L., 2015. Unconformities and their influence on lower Paleozoic petroleum reservoir development in the Tarim Basin. J. Pet. Sci. Eng. 133, 335–351.
Gao, Z.Q., Fan, T.L., Ding, Q.N., Hu, X.L., 2016. A third-order unconformity within lower ordovician carbonates in the Tarim Basin, NW China: Implications for reservoir development. J. Pet. Geol 39 (3), 287–304.
Geyer, G., Bayet-Goll, A., Wilmsen, M., Mahboubi, A., Moussavi Harami, S.R., 2014. Lithostratigraphic revision of the middle Cambrian (Series 3) and upper Cambrian (Furongian) in northern and central Iran. Newsletter Strtaigr. 47, 21–59.
Geyer, G., Shergold, J., 2000. The quest for internationally recognized divisions of Cambrian time. Episodes J. Int. Geosci. 23 (3), 188–195.
Gill, B.C., Lyons, T.W., Saltzman, M.R., 2007. Parallel, high-resolution carbon and sulphur isotope records of the evolving Paleozoic marine sulphur reservoir. Palaeogeogr. Palaeoclimatol. Palaeoecol. 256 (3–4), 156–173.
Gill, B.C., Lyons, T.W., Young, S.A., Kump, L.R., Knoll, A.H., Saltzman, M.R., 2011. Geochemical evidence for widespread euxinia in the Later Cambrian ocean. Nature 469 (7328), 80–83.
Glumac, B., Spivak-Birndorf, M.L., 2002. Stable isotopes of carbon as an invaluable stratigraphic tool: an example from the Cambrian of the northern Appalachians, USA. Geology 30 (6), 563–566.
Golonka, J., 2009. Phanerozoic paleoenvironment and paleolithofacies maps. Early Paleozoic. Geologia/Akademia Górniczo-Hutnicza im. Stanisława Staszica w Krakowie 35, 589–654.
Gould, K.M., Piper, D.J., Pe-Piper, G., MacRae, R.A., 2014. Facies, provenance and paleo-climate interpretation using spectral gamma logs: Application to the Lower Cretaceous of the Scotian Basin. Mar. Pet. Geol. 57, 445–454.
Guo, Q.J., Deng, Y., Hu, J., Wang, L.Y., 2017. Carbonate carbon isotope evolution of seawater across the Ediacaran-Cambrian transition: evidence from the Keping area, Tarim Basin, NW China. Geol. Magazine 154 (6), 1244–1256.
Haq, B.U., Schutter, S.R., 2008. A chronology of Paleozoic sea-level changes. Science 322 (5898), 64–68.
He, Z.L., Gao, Z.Q., Zhang, J.T., 2014. Types of sequence boundaries and their control over formation and distribution of quality carbonate reservoirs. Oil Gas Geol. 35 (6), 853–859.
He, J.Y., Qing, H.R., Xu, B., 2019. The unconformity-related palaeokarst in the uppermost Ediacaran carbonate rocks in the northwestern Tarim Block, NW China: implication for sedimentary evolution during the Ediacaran-Cambrian transition. Int. Geol. Rev. 61 (7), 839–852.
Hintze, L.F., Robison, R.A., 1975. Middle Cambrian stratigraphy of the House, Wah Wah, and adjacent ranges in western Utah. Geol. Soc. Am. Bull. 86 (7), 881–891.
Huang, Y., Fan, T.L., Berra, F., 2020. Architecture and paleogeography of the Early Paleozoic carbonate systems in the east-central Tarim Basin (China): constraints from seismic and well data. Mar. Pet. Geol. 113, 104147.
Hurtgen, M.T., Pruss, S.B., Knoll, A.H., 2009. Evaluating the relationship between the carbon and sulfur cycles in the later Cambrian ocean: an example from the Port au Port Group, western Newfoundland, Canada. Earth Planetary Sci. Lett. 281 (3–4), 288–297.
Jacobi, R.D., Mitchell, C.E., 2002. Geodynamical interpretation of a major unconformity in the Taconic Foredeep: Slide scar or onlap unconformity? Phys. Chem. Earth Parts A/B/C 27 (1–3), 169–201.
Jacobsen, S.B., Kaufman, A.J., 1999. The Sr, C and O isotopic evolution of Neoproterozoic seawater. Chem. Geol. 161 (1–3), 37–57.
Jadoon, Q.K., Roberts, E., Blenkinsop, T., Raphael, A.J., Shah, S.A., 2016. Mineralogical modelling and petrophysical parameters in Permian gas shales from the Roseneath and Murteree formations, Cooper Basin, Australia. Petroleum Explor Dev 43 (2), 277–284.
Jiang, M.S., Zhu, J.Q., Chen, D.Z., Qiao, G.S., 2001. Carbon and strontium isotope variations and responses to sea-level fluctuations in the Ordovician of the Tarim Basin. Sci. China Ser. D Earth Sci. 44 (9), 816–823.
Jing, X.C., Deng, S.H., Zhao, Z.J., Lu, Y.Z., Zhang, S.B., 2008. Carbon isotope composition and correlation across the Cambrian-Ordovician boundary in Kalpin Region of the Tarim Basin, China. Sci. China Ser. D Earth Sci. 51 (9), 1317–1329.
Kaufman, A.J., Jacobsen, S.B., Knoll, A.H., 1993. The Vendian record of Sr and C isotopic variations in seawater: implications for tectonics and paleo-climate. Earth Planet. Sci. Lett. 120 (3–4), 409–430.
Kaufman, A.J., Knoll, A.H., 1995. Neoproterozoic variations in the C-isotopic composition of seawater: stratigraphic and biogeochemical implications. Precambr. Res. 73 (1), 27–49.
Kouchinsky, A., Bengtson, S., Gallet, Y., Korovnikov, I., Pavlov, V., Runnegar, B., Shields, G., Veizer, J., Young, E., Ziegler, K., 2008. The SPICE carbon isotope excursion in Siberia: a combined study of the upper Middle Cambrian-lowermost Ordovician Kulyumbe River section, northwestern Siberian Platform. Geol. Mag. 145 (5), 609–622.
Lee, J., Chen, J., Chough, S.K., 2015. The middle–late Cambrian reef transition and related geological events: a review and new view. Earth Sci. Rev. 145, 66–84.
Li, R.W., Chen, J.S., Chen, Z.M., 2000. Characteristics of the C-and O-isotopic compositions of carbonates in the weathering profile at the unconformable boundary between the early cambrian and late Proterozoic in Ji County, North China. Chin. J. Geol. (Scientia Geologica Sinica) 35 (1), 55–59.
Li, C., Jin. C., Planavsky, N, J., Algeo, T, J., Cheng, M., Yang. X.L., Zhao, Y.L., Xie, S.C., 2017b. Coupled oceanic oxygenation and metazoan diversification during the early-middle Cambrian?. Geology, 45(8), 743-746.
Li, S.H., Li, S.P., Hu, Y.Y., Wu, W., Liu, B., Li, Z.T., 2017b. Sequence stratigraphy: problems and discussion. Earth Sci. 42 (12), 2312–2326.
Li, D.S., Liang, D., Jia, C.Z., Wang, G., Wu, Q.Z., He, D.F., 1996. Hydrocarbon Accumulations in the Tarim Basin, China. AAPG Bull. 80 (10), 1587–1603.
Li, H., Wang, J., Yin, J.Y., 2007. Method of identifying unconformity by using logging data. Geophys. Prospect. Petrol. (in Chinese) 46 (4), 421–424.
Li, J.H., Wang, H.H., Li, W.B., Zhou, X.B., 2014. Discussion on global tectonics evolution from plate reconstruction in Phanerozoic. Acta Pet. Sin. 35 (2), 207–218.
Li, J.H., Zhou, X.B., Li, W.B., Wang, H.H., Liu, Z.L., Zhang, H.T., Taskyn, A., 2015. Preliminary Reconstruction of Tectonic Paleogeography of Tarim Basin and Its Adjacent Aeras from Cambrian to Triassic, NW China. Geol. Rev. 61 (6), 1225–1234.
Lin, C.S., Yang, H.J., Liu, J.Y., Peng, L., Cai, Z.Z., Yang, X.F., Yang, Y.H., 2009. Paleostructural geomorphology of the Paleozoic central uplift belt and its constraint on the development of depositional facies in the Tarim Basin. Sci. China Ser. D Earth Sci. 52 (6), 823–834.
Lin, C.S., Yang, H.J., Liu, J.Y., Rui, Z., Cai, Z., Zhu, Y., 2012. Distribution and erosion of the Paleozoic tectonic unconformities in the Tarim Basin, Northwest China: significance for the evolution of paleo-uplifts and tectonic geography during deformation. J. Asian Earth Sci. 46, 1–19.
Lindsay, J.F., Kruse, P.D., Green, O.R., Hawkins, E., Brasier, M.D., Cartlidge, J., Corfield, R.M., 2005. The Neoproterozoic-Cambrian record in Australia: a stable isotope study. Precambr. Res. 143 (1–4), 113–133.
Liu, H., Liao, Z.W., Zhang, H.Z., Tian, Y.K., Cheng, B., Yang, S., 2017. Stable isotope (δ13Cker, δ13Ccarb, δ18Ocarb) distribution along a Cambrian outcrop section in the eastern Tarim Basin, NW China and its geochemical significance. Geosci. Front. 8 (1), 163–170.
Liu, J.Y., Lin, C.S., Peng, L., Chen, Q.Q., Zhang, X.X., Zhou, X.J., 2008. Distribution patterns of the end of the middle devonian tectonic unconformity and their constrain on the development and distribution of favorable stratigraphic traps in the tarim basin. Oil Gas Geol. (in Chinese with English Abstract) 29 (2), 268–275.
Liu, H., Somerville, I.D., Lin, C., Zuo, S.J., 2016. Distribution of Palaeozoic tectonic superimposed unconformities in the Tarim Basin, NW China: significance for the evolution of palaeogeomorphology and sedimentary response. Geol. J. 51 (4), 627–651.

Maruyama, S., Sawaki, Y., Ebisuzaki, T., Ikoma, M., Omori, S., Komabayashi, T., 2014. Initiation of leaking Earth: an ultimate trigger of the Cambrian explosion. Gondw. Res. 25 (3), 910–944.
McKenzie, N.R., Hughes, N.C., Myrow, P.M., Choi, D.K., Park, T.Y., 2011. Trilobites and zircons link north China with the eastern Himalaya during the Cambrian. Geology 39 (6), 591–594.
Miller, K.G., Kominz, M.A., Browning, J.V., Wright, J.D., Mountain, G.S., Katz, M.E., Sugarman, P.J., Cramer, B.S., Christie-Blick, N., Pekar, S.F., 2005. The Phanerozoic record of global sea-level change. Science 310 (5752), 1293–1298.
Miller, K.B., West, R.R., 1998. Identification of sequence boundaries within cyclic strata of the Lower Permian of Kansas, USA: problems and alternatives. J. Geol. 106 (2), 119–132.
Miriam, C., Vincen, P., 2000. Sedimentary and biological response to sea level and paleaoceanographic changes of a Low Middle Jurassic Tethyan platform margin (Southern Alps, Italy). Palaeogeogr. Palaeoclimatol. Palaeoecol 169, 219.
Montañez, I.P., Osleger, D.A., Banner, J.L., Mack, L.E., Musgrove, M., 2000. Evolution of the Sr and C isotope composition of Cambrian oceans. GSA Today 10 (5), 1–7.
Morgan, W.A., 2013. Sequence Stratigraphy of the Great American Carbonate Bank. In: Derby, J.R., Fritz, R.D., Longacre, S.A., Morgan, W.A., Sternbach, C.A. (Eds.), The Great American Carbonate Bank: The Geology and Economic Resources of the Cambrian–Ordovician Sauk Megasequence of Laurentia. AAPG Memoir 98. AAPG, 37–82.
Myers, K.J., Bristow, C.S., 1989. Detailed sedimentology and gamma-ray log characteristics of a Namurian deltaic succession II: gamma-ray logging. Geol. Soc. Lond Special. Publ. 41 (1), 81–88.
Ng, T.W., Yuan, J.L., Lin, J.P., 2014. The North China Steptoean positive carbon isotope excursion and its global correlation with the base of the Paibian Stage (early Furongian Series), Cambrian. Lethaia 47 (2), 153–164.
Ngia, N.R., Hu, M.Y., Gao, D., Hu, Z.G., Sun, C.Y., 2019. Application of stable strontium isotope geochemistry and fluid inclusion microthermometry to studies of dolomitization of the deeply buried Cambrian carbonate successions in west-central Tarim Basin, NW China. J. Earth Sci. 30 (1), 176–193.
Nishidai, T., Berry, J.L., 1990. Structure and hydrocarbon potential of the Tarim Basin (NW China) from satellite imagery. J. Pet. Geol 13 (1), 35–58.
Palmer, A.R., 1981. Subdivision of the Sauk Sequence. In: Taylor, M.E. (Ed.), Short Papers for the Second International Symposium on the Cambrian System. U.S. Geological Survey, Open-file Report 81-743, 160–162.
Pan, W.Q., Chen, Y.Q., Xiong, Y.X., Li, B.H., Xiong, R., 2015. Sedimentary facies research and implications to advantaged exploration regions on Lower Cambrian source rocks, Tarim Basin. Natural Gas Geosci. 26 (7), 1224–1232.
Park, T.Y., Choi, D.K., 2011. Trilobite faunal successions across the base of the Furongian Series in the Taebaek Group, Taebaeksan Basin, Korea. Geobios 44 (5), 481–498.
Park, T.Y., Kihm, J.H., Choi, D.K., 2013. Late middle Cambrian (Cambrian Series 3) trilobite faunas from the lowermost part of the Sesong Formation, Korea and their correlation with North China. J. Paleo. 87 (6), 991–1003.
Peng, S.C., 2009. Review on the studies of Cambrian trilobite faunas from Jiangnan Slope Belt, South China, with notes on Cambrian correlation between South and North China. Acta Palaeontol. Sin. 48 (3), 437–452.
Peng, S.C., Babcock, L., Robison, R., Lin, H.L., Rees, M., Saltzman, M., 2004a. Global standard stratotype-section and point (GSSP) of the Furongian Series and Paibian Stage (Cambrian). Lethaia 37 (4), 365–379.
Peng, S.C., Babcock, L.E., Zuo, J.X., Lin, H.L., Zhu, X.J., Yang, X.F., Saltzman, M.R., Robison, R.A., Qi, Y.P., Bagnoli, G., Chen, Y., 2004b. The Global Boundary Stratotype Section and Point (GSSP) of the Guzhangian Stage (Cambrian) in the Wuling Mountains, Northwestern Hunan, China. Episodes 32 (1), 41–55.
Peng, S.C., Babcock, L.E., Geyer, G., Moczydlowska, M., 2006. Nomenclature of Cambrian epochs and series based on GSSPs - Comments on an alternative proposal by Rowland and Hicks. Episodes 29 (2), 130–132.
Peng, S.C., Babcock, L.E., Cooper, R.A., 2012. The Cambrian Period. In: Gradstein, F.M., Ogg, J.G., Schmitz, M., Ogg, G. (Eds.), The Geologic Time Scale 2012. Elsevier, pp. 437–488.
Qing, H., Veizer, J., 1994. Oxygen and carbon isotopic composition of Ordovician brachiopods: Implications for coeval seawater. Geochim. Cosmochim. Acta 58 (20), 4429–4442.
Robison, R.A., 1982. Some Middle Cambrian agnostoid trilobites from western North America. J. Paleo. 56, 132–160.
Robison, R.A.,1999. Base of Ptychagnostus atavus Zone, candidate stratotype for base of unnamed international series, in Palmer, A.R., ed., Laurentia 99. V Field Conference of the Cambrian Stage Subdivision Working Group, International Subcommission on Cambrian Stratigraphy, Institute for Cambrian Studies, Boulder, Colorado, pp. 15–17.
Rush, P.F., Chafetz, H.S., 1990. Fabric-retentive, non-luminescent brachiopods as indicators of original delta 13C and delta 18O composition; a test. J. Sediment. Res. 60 (6), 968–981.
Saller, A.H., Budd, D.A., Harris, P.M., 1994. Unconformities and porosity development in carbonate strata: ideas from a Hedberg conference. AAPG Bull. 78 (6), 857–872.
Saltzman, M.R., Runnegar, B., Lohmann, K.C., 1998. Carbon isotope stratigraphy of Upper Cambrian (Steptoean Stage) sequences of the eastern Great Basin: record of a global oceanographic event. Geol. Soc. Am. Bull. 110 (3), 285–297.
Saltzman, M.R., Ripperdan, R.L., Brasier, M.D., Lohmann, K.C., Robinson, R.A., Chang, W.T., Peng, S.C., Ergaliev, E.K., Runnegar, B., 2000. A global carbon isotope excursion (SPICE) during the Late Cambrian: relation to trilobite extinctions, organicmatter burial and sea level. Palaeogeogr. Palaeoclimatol. Palaeoecol. 162 (3–4), 211–223.
Saltzman, M.R., Cowan, C.A., Runkel, A.C., Runnegar, B., Stewart, M.C., Palmer, A.R., 2004. The Late Cambrian SPICE (δ13C) event and the Sauk II-Sauk III regression: new evidence from Laurentian basins in Utah, Iowa, and Newfoundland. J. Sediment. Res. 74 (3), 366–377.
Saltzman, M.R., Young, S.A., Kump, L.R., Gill, B.C., Lyons, T.W., Runnegar, B., 2011. Pulse Of Atmospheric oxygen during the late Cambrian. Proceedings of the National Academy of Sciences, 108(10), 3876-3881.
Shahkarami, S., Buatois, L.A., Mángano, M.G., Hagadorn, J.W., Almond, J., 2020. The Ediacaran-Cambrian boundary: evaluating stratigraphic completeness and the Great Unconformity. Precambr. Res. 345, 105721.
Shi, K.B., Liu, B.o., Tian, J.C., Pan, W.Q., 2016. Sedimentary characteristics and lithofacies paleogeography of Sinian in Tarim Basin. Acta Pet. Sin. 37 (11), 1343.
Shi, K.B., Liu, B., Jiang, W.M., Luo, Q.Q., Gao, X.Q., 2018. Nanhua-Sinian tectono-sedimentary framework of Tarim Basin, NW China. Oil Gas Geology 39 (5), 862–877.
Sial, A.N., Peralta, S., Ferreira, V.P., Toselli, A.J., Aceñolaza, F.G., Parada, M.A., Gaucher, C., Alonso, R.N., Pimentel, M.M., 2008. Upper Cambrian carbonate sequences of the Argentine Precordillera and the Steptoean C-Isotope positive excursion (SPICE). Gondw. Res. 13 (4), 437–452.
Sial, A.N., Peralta, S., Gaucher, C., Toselli, A.J., Ferreira, V.P., Frei, R., Parada, M.A., Pimentel, M.M., Pereira, N.S., 2013. High-resolution stable isotope stratigraphy of the upper Cambrian and Ordovician in the Argentine Precordillera: carbon isotope excursions and correlations. Gondw. Res. 24 (1), 330–348.
Tang, L.J., 1994. Evolution and Tectonic Patterns of Tarim Basin. Earth Science-J. China Univ. Geosci. 19 (6), 742–754.
Tang, L.J., 1997. Major evolutionary stages of Tarim Basin in Phanerozoic time. Earth Sci. Front. 4 (3–4), 318–324.
Tang, L.J., Qi, L.X., Qiu, H.J., Yun, L., Li, M., Xie, D.Q., Yang, Y., Wan, G.M., 2012. Polyphase differential fault movement and hydrocarbon accumulation of the Tarim Basin, NW China. Acta Petrologica Sinica 28 (8), 2569–2583.
Tian, L., Cui, H.F., Liu, J., Zhang, N.C., Shi, X.Q., 2018. Early-Middle Cambrian paleogeography and depositional evolution of Tarim Basin. Oil Gas Geol. 39 (5), 1011–1021.
Tian, L., Zhang, H.Q., Liu, J., Zhang, N.C., Shi, X.Q., 2020. Distribution of Nanhua-Sinian rifts and proto-type basin evolution in southwestern Tarim Basin, NW China. Petrol. Explorat. Devel. 47 (6), 1122–1133.
Van Wagoner, J.C., Mitchum, R.M., J R., C Ampion, K.M., Rahmanian, V.D., 1990, Siliciclastic sequence stratigraphy in well logs, cores, and outcrops: American Association Petroleum Geologists, Methods in Exploration Series 7, 55.
Veizer, J., Ala, D., Azmy, K., Bruckschen, P., Buhl, D., Bruhn, F., Carden, G.A.F., Diener, A., Ebneth, S., Godderis, Y., Jasper, T., Korte, C., Pawellek, F., Podlaha, O., Strauss, H., 1999. 87 Sr/ 86 Sr, δ13C and δ18O evolution of Phanerozoic seawater. Chem. Geol. 161 (1–3), 59–88.
Wang, Y., 1999. Sequence Stratigraphy of the Sinian-Middle Devonian System in the Tarim Basin. Acta Sedimentol. Sin. 17, 414–421.
Wang, D.R., Feng, X.J.,2002. Research on Carbon and Oxygen Geochemistry of Lower Paleozoic in North China. Acta Geologica Sinica. Acta Geologica Sinica, 2002, 76(3): 400- 408.
Wang, H.Y., Gao, Z.Q., Machel, H.G., Fan, T.L., Wei, D., 2017b. The Cambrian-Ordovician boundary in the Tarim Basin, NW China: Geochemistry and geophysics data anomalies. J. Pet. Sci. Eng. 156, 497–512.
Wang, L.Y., Guo, Q.J., Zhao, C.Q., Wei, R.F., Deng, Y.N., Han, X.K., Tian, L.Y., Kong, J., Yang, X., 2020b. Trace and rare earth elements geochemistry of sedimentary rocks in the Ediacaran-Cambrian transition from Tarim Basin, Northwest China: Constraints for redox environments. Precambr. Res. 352, 105942.
Wang, X.L., Hu, W.X., Yao, S.P., Chen, Q., Xie, X.M., 2011. Carbon and strontium isotopes and global correlation of Cambrian Series 2-Series 3 carbonate rocks in the Keping area of the northwestern Tarim Basin, NW China. Marine Petrol. Geol. 28 (5), 992–1002.
Wang, H.Z., Liu, H., Wei, Z.W., Deng, Q., Li, S.D., Zhang, H.Z., Cheng, B., Liao, Z.W., 2020a. Determination of SPICE event from the upper Cambrian strata and its geochemical significance in the eastern Tarim Basin, NW China. J. Nanjing Univ. (Natural Science) 56 (3), 354–365.
Wang, G., Wang, J., Wang, Z., Chen, C., Yang, J.X., 2017a. Carbon isotope gradient of the Ediacaran cap carbonate in the Shennongjia area and its implications for ocean stratification and palaeogeography. J. Earth Sci. 28 (2), 187–195.
Wignall, P.B., Twitchett, R.J., 1996. Oceanic anoxia and the end Permian mass extinction. Science 272 (5265), 1155–1158.
Woods, M.A., Wilby, P.R., Leng, M.J., Rushton, A.W., Williams, M., 2011. The furongian (late Cambrian) steptoean positive carbon isotope excursion (SPICE) in avalonia. J. Geol. Soc. London 168 (4), 851–862.
Wotte, T., Álvaro, J.J., Shields, G.A., Brown, B., Brasier, M.D., Veizer, J., 2007. C-, O- and Sr-isotope stratigraphy across the Lower-Middle Cambrian transition of the Cantabrian Zone (Spain) and the Montagne Noire (France), West Gondwana. Palaeogeogr. Palaeoclimatol. Palaeoecol. 256 (1–2), 47–70.
Wotte, T., Strauss, H., 2015. Questioning a widespread euxinia for the Furongian (Late Cambrian) SPICE event: indications from δ13C, δ18O, δ34S and biostratigraphic constraints. Geol. Mag. 152 (6), 1085–1103.
Wu, Y.S., Wang, W., Jiang, H.X., Cui, Y., Zhao, R., Huang, Z.B., Yang, Z.B., Chen, Y.Q., 2021. Evolution patterns of seawater carbon isotope composition during the Cambrian and their stratigraphic significance. Geol. J. 56 (1), 457–474.
Xu, Z.Q., Li, S.T., Zhang, J.X., Yang, J.S., He, B.Z., Li, H.B., Lin, C.S., Cai, Z.H., 2011. Paleo-Asian and Tethyan tectonic systems with docking the Tarim b, lock. Acta Petrol. Sin. 27 (1), 1–22.
Yang, H.J., Chen, Y.Q., Pan, W.Q., Wang, B., Yang, W.J., Huang, S.Y., Yang, P.F., Yi, Y., Wang, X.X., 2021a. Study on tectonic and sedimentary evolution during the Nanhua-Middle Cambrian and its significance for subsalt exploration, Tarim Basin. China Petroleum Exploration 26 (4), 84–98.

Yang, X.Q., Li, Z., Gao, B., Zhou, Y.Q., 2021b. The Cambrian Drumian carbon isotope excursion (DICE) in the Keping area of the northwestern Tarim Basin, NW China. Palaeogeogr. Palaeoclimatol. Palaeoecol. 571, 110385.
Yao, C.Y., Ding, H.F., Ma, D.S., Li, G.X., 2014. Carbon Isotope Features of the Sugetbrak Section in the Aksu—Wushi Area, Northwest China: Implications for the Precambrian/Cambrian Stratigraphic Correlations. Acta Geologica Sinica-English Edition 88 (5), 1535–1546.
Zhang, S., Huang, H., 2005. Geochemistry of Palaeozoic marine petroleum from the Tarim Basin, NW China: Part 1. Oil family classification. Organic Geochem. 36 (8), 1204–1214.
Zhang, G.Y., Song, J.G., 1998. Control of basin reworking on hydrocarbon accumulation and preservation in the Tarim cratonic basin, Northwest China. Geol. Rev. 44 (5), 511–521.
Zhang, Y.G., Yang, T., Hohl, S.V., Zhu, B., He, T.C., Pan, W.Q., Chen, Y.Q., Yao, X.Z., Jiang, S.Y., 2020. Seawater carbon and strontium isotope variations through the late Ediacaran to late Cambrian in the Tarim Basin. Precambr. Res. 345, 105769.
Zhang, S.G., 1985. Stratigraphic division and faunal characteristics of the Cambrian in Kuluktag, Xinjiang. Proceedings of Xinjiang Geological Research, Volksverlag Xinjiang, 36-58.
Zhao, Z.J., 2015. Indicators of global sea-level change and research methods of marine tectonic sequences:take Ordovician of Tarim Basin as an example. Acta Pet. Sin. 36 (3), 262–273.
Zheng, H.R., Wu, M.B., Wu, X.W., Zhang, T., Liu, C.Y., 2007. Oil–gas exploration prospect of dolomite reservoir in the Lower Paleozoic of Tarim Basin. Acta Pet. Sin. 28 (2), 1.
Zhong, D., Hao, Y., 1990. Sinian to Permian Stratigraphy and Palaeontology of the Tarim Basin, Xinjiang, (I) Kuruktag Region (in Chinese withEnglish abstract). Nanjing University Press, Nangjin, pp. 1–252.
Zhou, Z.Y., 2001. Stratigraphy of the Tarim Basin (in Chinese with English abstract). Science Press, Beijing, p. 359.
Zhou, Z., Chen, P., 1990. Biostratigraphy and Geological Evolution of Tarim (in Chinese). Science Press, Beijing.
Zhu, M.Y., Zhang, J.M., Li, G.X., Yang, A.H., 2004. Evolution of C isotopes in the Cambrian of China: implications for Cambrian subdivision and trilobite mass extinctions. Geobios 37 (2), 287–301.
Zhu, M.Y., Babcock, L.E., Peng, S.C., 2006. Advances in Cambrian stratigraphy and paleontology: Integrating correlation techniques, paleobiology, taphonomy and paleoenvironmental reconstruction. Palaeoworld 15 (3–4), 217–222.
Zhu, Y.J., Shen, A.J., Liu, L.L., Chen, Y.Q., Yu, G., 2019b. Tectonic-sedimentary filling history through later Sinian to mid-Cambrian in Tarim Basin and its explorational potential. Acta Sedimentologica Sinica (Chenji Xuebao) 38, 1–14.
Zhu, M.Y., Yang, A.H., Yuan, J.J., Li, G.X., Zhang, J.M., Zhao, F.C., Ahn, S., Miao, L.Y., 2019a. Cambrian integrative stratigraphy and timescale of China. Sci. China Earth Sci. 62 (1), 25–60.
Zuo, J.X., Peng, S.C., Qi, Y.P., Zhu, X.J., Bagnoli, G., Fang, H.B., 2018. Carbon-Isotope Excursions Recorded in the Cambrian System, South China: Implications for Mass Extinctions and Sea-Level Fluctuations. J. Earth Sci. 29 (3), 479–491.
Zuo, J.X., Zhu, X.J., Fang, H.B., Chen, Y.L., 2020. Carbon Isotope Trend across the Base of Furongian Series of Cambrian, Northern Henan, North China. Earth Sci. 45 (3), 728–738.

Further reading

Chen, Y.Q., Zhang, Y.Q., Wu, Y.S., Zhou, P., Li, K.K., Wang, X.X., 2020a. Discovery of SPICE and carbon isotope stratigraphic correlation of the Cambrian Furongian Series in Tarim Craton, NW China. Science China Earth Sci. 63 (9), 1330–1338.
Li, D.D., Zhang, X.L., Zhang, X., Zhu, H., Peng, S.C., Sun, L.L., Shen, Y.N., 2020. A paired carbonate–organic δ13C approach to understanding the Cambrian Drumian carbon isotope excursion (DICE). Precambr. Res. 349, 105503.